Mathematics in Applied Sciences and Engineering
Volume **5**, Number **2**, June **2024**, pp.**120-148**
https://ojs.lib.uwo.ca/mase
https://doi.org/10.5206/mase/17134

UNRAVELING THE ROLE OF INERT BIOMASS IN MEMBRANE AERATED BIOFILM REACTORS FOR SIMULTANEOUS NITRIFICATION AND DENITRIFICATION

MARYAM GHASEMI, SHENG CHANG, AND SIVABAL SIVALOGANATHAN

Abstract. This study presents an innovative 2D spatio-temporal model that sheds light on the intricate formation of biofilms, incorporating two essential biomass decay pathways: cell lysis and endogenous respiration. The model encompasses heterotrophic bacteria (HB), anaerobic heterotrophic bacteria (AHB), and autotrophic bacteria (AB), offering a comprehensive understanding of multi-species biofilm development. Through meticulous simulations, we explore the primary mechanisms behind inert biomass formation in biofilms, revealing the key roles played by the lysis of HB, AHB, and AB, as well as the endogenous respiration of HB. Moreover, the simulations reveal how species of higher abundance contribute significantly to inert biomass generation, reshaping our understanding of biofilm dynamics. Crucially, this study highlights the indispensability of considering biofilm inert biomass when modeling the nitrification and denitrification behaviors of a membrane aerated biofilm reactor (MABR). The distribution of oxygen and acetate across biofilm thickness is remarkably different when inert biomass is factored in, underscoring the necessity for a more holistic approach to modeling biofilm behavior. With the introduction of the inert biomass inclusive biofilm model, our simulations explore the interactive effects of key process conditions - bulk concentrations of oxygen (O_∞), ammonium nitrogen ($N_{1\infty}$), acetate (A_∞), and biofilm thickness - on the nitrification and denitrification performance of MABR. A compelling correlation emerges between higher bulk concentrations of oxygen and ammonium nitrogen and optimal nitrification rates, achieving an impressive range of 0.3 to 1.1g ammonium/m^2/d. Delving into denitrification, we observe that high O_∞, low $N_{1\infty}$, and either high or low A_∞ levels impede AHB formation and consequently hinder denitrification. Our findings provide a roadmap for achieving simultaneous nitrification and denitrification, contingent on specific conditions: $10[gm^{-3}] < O_\infty < 15[gm^{-3}]$, $12[gm^{-3}] < N_{1\infty} < 20[gm^{-3}]$, A_∞ ranging from $3[gm^{-3}]$ to $12[gm^{-3}]$, and a biofilm thickness $> 1.4[mm]$. While our study reveals promising avenues for simultaneous nitrification and denitrification, denitrification rates still lag behind nitrification rates under the same conditions. As a result, we advocate for further investigations to devise strategies that can enhance denitrification in MABR systems. In conclusion, this study advances our knowledge of biofilm dynamics by introducing a comprehensive model and illuminating the key factors driving nitrification and denitrification performance in MABRs. These findings pave the way for improved biofilm engineering and wastewater treatment strategies, opening new horizons for sustainable environmental practices.

1. Introduction

Wastewater pollution from domestic, commercial, public service, industrial, and agricultural sources has become a global environmental challenge, severely affecting the quality of water bodies such as

Received by the editors 28 November 2023; accepted 10 March 2024; published online 26 March 2024.
2020 *Mathematics Subject Classification.* 35K65, 65N08, 34C60, 65L05, 68U20, 92D25.
Key words and phrases. Nitrification-denitrification, biofilm, membrane aerated bioreactor, inert biomass, nonlinear diffusion-reaction model, cross-diffusion.
SS acknowledges the support received from the Natural Sciences and Engineering Research Council of Canada (NSERC) through Discovery Grant #RGPIN-04771-2014.

rivers and ultimately impacting the health of humans and animals [50]. To address these pressing concerns caused by wastewater pollution, a variety of advanced technologies have been implemented, including membrane aerated biofilm reactors (MABRs), which hold the potential to efficiently remove both organic and inorganic contaminants from wastewater. MABRs offer a unique counter-diffusion mass transfer mechanism, enabling the simultaneous supply of carbonaceous and nitrogenous substrates, along with oxygen, from opposite sides of the biofilm. This makes MABRs particularly promising for achieving simultaneous nitrification and denitrification (SND) in wastewater treatment with low carbon to nitrogen (C:N) ratios [9, 25, 28, 29, 43]. A key distinguishing characteristic of MABRs from conventional biofilm-based wastewater treatment technologies such as trickling filter, rotating biological contactor, and fixed or moving bed biofilm reactors [38] is the precise control over oxygen supply to biofilms through oxygen-permeable membranes. This feature allows for the creation of biofilms at the membrane surface, leading to a high dissolved oxygen (DO) profile in the inner layers of the biofilm close to the membrane. In this oxygen-rich region, nitrification bacteria flourish that effectively oxidize NH_4^+ to NO_2^- or NO_3^-. Simultaneously, aerobic heterotrophic bacteria actively consume biochemical oxygen demand (BOD) and contribute to the overall treatment efficiency. As oxygen concentrations decrease towards the outer surface of the biofilm, an anoxic zone is established, promoting the growth of anaerobic heterotrophic bacteria that are responsible for denitrification or reduction of NO_2^- or NO_3^- to nitrogen gas. This dynamic interplay gives rise to stratified biofilm layers, enabling the simultaneous removal of BOD, nitrification, and denitrification within MABR reactors [20, 32].

Achieving optimal SND performance in MABRs in terms of maintaining a high-level of total nitrogen removal with minimum oxygen and carbon consumption requires a thorough understanding of critical factors that influence the process. These factors include biofilm thickness, oxygen concentration, C:N ratio, and hydraulic retention time (HRT) [5, 7, 25, 33, 35, 44, 47]. An essential aspect often overlooked in realistic MABR performance descriptions is the gradual loss of active biomass over time and the accumulation of inert biomass. This phenomenon arises from various processes, including cell detachment, decay, lysis, and endogenous respiration [49]. Endogenous respiration involves the consumption of intracellular materials, such as glycogen or polyhydroxy-alkanoate, in the absence of external substrate [12]. Part of the decayed biomass through respiration is slowly biodegradable substance that is used to yield energy for maintenance while the remaining is non-biodegradable and form residual inert biomass [26]. The decay/lysis concept, known as death-regeneration, also involves the decay of cells and subsequent consumption of fraction of the decayed biomass as a substrate for the growth of new biomass [48]. In activated sludge process models like IAWQ, ASM1, and ASM2, loss of active biomass is commonly described based on endogenous respiration and cell decay/lysis concepts, with the non-biodegradable fraction of dead cell debris remaining in the mixed liquor as inert biomass [26, 48]. In MABR systems, the inert biomass generated through these pathways remains within the biofilm, potentially exerting a more significant impact on process performance compared to suspended activated sludge systems. Although inert biomass within biofilms does not consume substrate, it can act as a barrier, influencing substrate transformation within the biofilm and its development. Neglecting the effects of inert biomass may lead to overestimation of biofilm capacity in nitrogen removal or underestimation of nitrogen resources within the biofilm. Therefore, it is crucial to incorporate inert biomass accumulation and its impact in biofilm models for an accurate description of MABR performance. Decay of biomass through lysis and endogenous respiration and its effect on nitrogen removal have been considered separately in some theoretical studies [2, 8, 13, 30, 33, 49] showing that inert biomass affects the performance of MABRs noticeably. Nevertheless, formation of inert biomass through both pathways and its effect on the SND have not been studied particularly via spatio temporal multi-scale modeling, where the impact of inert biomass is more pronounced because volume filing effect is involved [10, 17].

To address this knowledge gap, our study aims to conduct a pioneering computational investigation of SND performance in MABRs under diverse environmental conditions, with a specific emphasis on the presence and role of inert biomass within the biofilm. Most mathematical models that have been proposed for computational study of the performance of MABRs and understanding the involved mechanisms are 1D models in which biofilm development is modeled in the framework of the 1D Wanner-Gujer model [49]. This model is constructed based on the implicit assumption that substrates and biomass components stratify completely. This is a good assumption for many well-developed biofilms with co-diffusional substrate supply that homogeneously cover the substratum. However, Ghasemi *et. al.* show in [19] that capturing biofilm development from a relatively realistic initial inoculum is possible only by utilizing higher dimensional models especially if internal structure of biofilm and substrate distribution within the biofilm are quantities of interest. Hence, leveraging a continuous, deterministic, 2D model, we delve into the spatial resolution of multi-species biofilms, offering comprehensive insights into inert biomass accumulation through both lysis and endogenous respiration. The main considerations to include cell lysis and endogenous respiration in simulating development of inert biomass are (1) both processes can result in accumulation of inactive biomass within biofilm, (2) the effect of these two mechanisms can vary with process conditions, and (3) inclusion of both mechanisms allows analyzing the effect of these two mechanisms on accumulation of inert biomass under different process conditions. This approach allows a holistic evaluation of the role of inert biomass in SND processes and optimizing total nitrogen removal with minimal oxygen and carbon consumption. Our research further investigates the formation of inert biomass through each decay pathway, distribution of inert biomass across biofilm thickness, and its consequential effect on SND performance. To the best of our knowledge, this is the first study that employs a higher dimensional partial differential equation (PDE) model to describe the development of a multi-species biofilm, comprising three distinct biomass types: autotrophs, heterotrophs, and inert biomass. This comprehensive modeling approach allows for a realistic evaluation of inert biomass impact on SND processes, particularly in the presence of volume filling effects. By understanding the hidden potential of inert biomass in MABRs, we can unlock a transformative era of enhanced SND performance, promising sustainable and efficient wastewater treatment solutions.

2. Mathematical model

To study the effect of formation of inert biomass on SND performance of a membrane aerated biofilm reactor (MABR), we develop the model introduced in [20] and include inert biomass as a particulate, i.e., volume occupying biomass fraction. To describe SND and the performance of MABR, we define computational domain $\Omega \subset \mathbb{R}^2$ as a rectangle of size $[0, L] \times [0, H]$ $[mm^2]$ which is divided into the biomass region in which the total biomass density (M) is positive, $\Omega_1(t) = \{(x, y) \in \Omega \subset \mathbb{R}^2 : \ M(t, x, y) > 0\}$ and the liquid phase (bulk liquid, channels and pores of a biofilm) where the biomass density is zero, $\Omega_2(t) = \{(x, y) \in \Omega \subset \mathbb{R}^2 : \ M(t, x, y) = 0\}$. As shown in Figure 1 these regions are separated by biofilm/liquid interface $\Gamma(t) = \partial\bar{\Omega}_1(t) \cap \partial\bar{\Omega}_2(t)$ which is not stationary and changes as time passes and biofilm grows. Moreover, neither Ω_1 nor Ω_2 need to be connected, and Γ can consist of several disjoint segments. To simulate an MABR and describe the nitrification/denitrification process we assume substratum is placed at the bottom boundary at which biofilm is formed and this segment of the computational domain also mimics the membrane through which oxygen is provided. Organic and inorganic nitrogen sources are added through the top boundary indicating the involvement of counter-diffusion mechanism, c.f. Figure 1. Biofilm is composed of four particulates: Inert biomass (I), autotrophic biomass (B_a), aerobic heterotrophic biomass (B_{h1}), and anaerobic heterotrophic biomass (B_{h2}). All these species are represented as volume fractions of maximum biomass density M_∞ i.e. $M_\infty \cdot (I, B_a, B_{h1}, B_{h2})[g/m^3]$ represent density of inert bacteria (I), autotrophic bacteria (AB), heterotrophic bacteria (HB), and anaerobic heterotrophic bacteria (AHB) respectively. As is common in mathematical models of biofilms, the EPS that is produced by the bacteria is subsumed in the biofilm

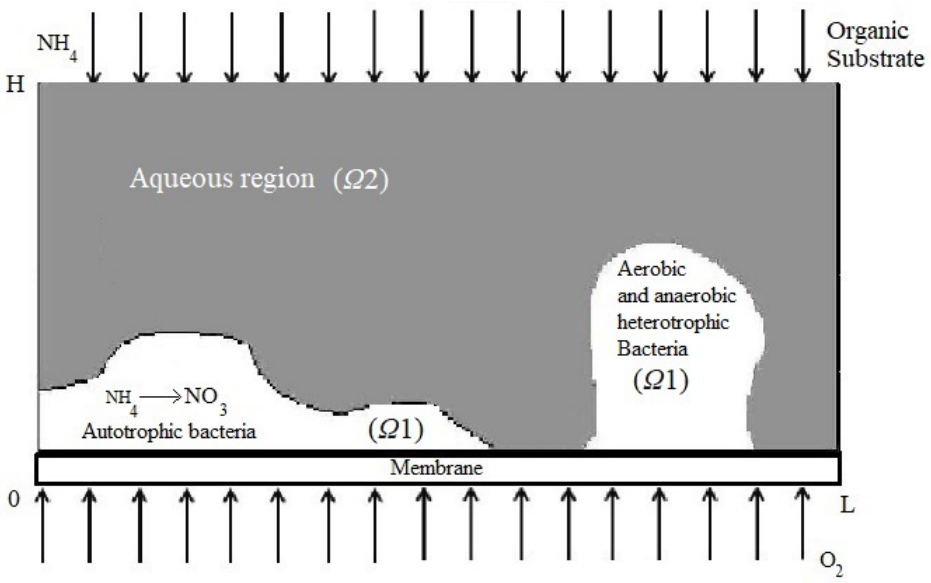

FIGURE 1. Schematic of the computational domain $\Omega \subset \mathbb{R}^2$ with liquid and biofilm region. The arrows show the direction of substrate fluxes through the boundaries.

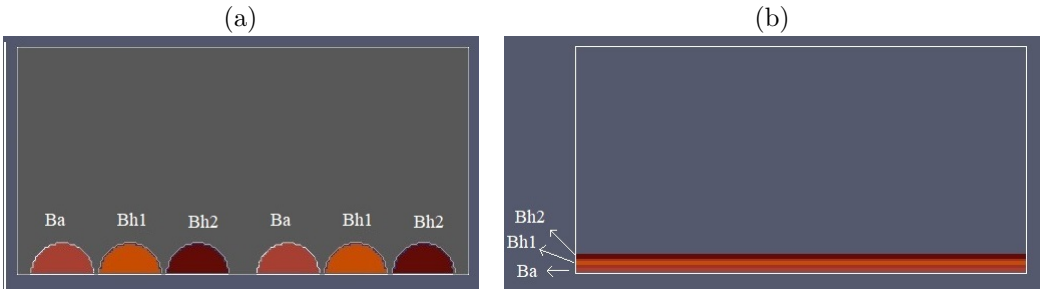

FIGURE 2. Initial coverage of the substratum for two scenarios. (a): heterogeneous inoculation including individual colonies of radius 160[μm]; (b): flat layer inoculation including layers of thickness 20[μm].

volume fraction. A biofilm model that accounts for EPS explicitly has been proposed, for example, in [15, 24, 26]. Decay of biomass through endogenous respiration produces slowly biodegradable and non-biodegradable substances. The biodegradable fraction of decayed biomass can be used to provide energy for maintenance through hydrolysis while the non-biodegradable fraction forms residual inert biomass that does not consume substrate and is not consumed by any reactions [26, 33, 34]. To avoid making the model more complex and since our focus in this study is on the effect of inert biomass on SND, we do not include slowly biodegradable fraction and hydrolysis in our model and take into account only the non-biodegradable fraction of decayed biomass. We also assume that all biomass loss through lysis is converted into residual inert biomass. Furthermore, it is assumed that inert biomass is removed physically or chemically. Nutrient substrates available in wastewater and required for biofilm growth are ammonium nitrogen, $N_1[gm^{-3}]$, nitrate nitrogen, $N_2[gm^{-3}]$, oxygen, $O[gm^{-3}]$, and acetate,

$A[gm^{-3}]$. Independent variables are time and spatial location denoted by $t \geq 0$ and $(x, y) \in \Omega$. Using these notations the model reads:

$$
\begin{cases}
\frac{\partial I}{\partial t} &= \nabla \cdot (\sum_{j=1}^{4} D_{1j}(\mathbf{M}) \nabla M_j) + \underbrace{f_d r_a \frac{O}{\kappa_{a_o} + O} B_a + f_d r_h \frac{O}{\kappa_{h_o} + O} B_{h1}}_{\text{R1}} \\
&\quad + \underbrace{d_a B_a + d_{h1} B_{h1} + d_{h2} B_{h2}}_{\text{R2}} \\
\frac{\partial B_a}{\partial t} &= \nabla \cdot (\sum_{j=1}^{4} D_{2j}(\mathbf{M}) \nabla M_j) + \underbrace{\mu_a \frac{O}{\kappa_{a_o} + O} \frac{N_1}{\kappa_{n1} + N_1} B_a}_{\text{R3}} - \underbrace{r_a \frac{O}{\kappa_{a_o} + O} B_a}_{\text{R1}} - \underbrace{d_a B_a}_{\text{R2}} \\
\frac{\partial B_{h1}}{\partial t} &= \nabla \cdot (\sum_{j=1}^{4} D_{3j}(\mathbf{M}) \nabla M_j) + \underbrace{\mu_h \frac{O}{\kappa_{h_o} + O} \frac{A}{\kappa_a + A} B_{h1}}_{\text{R4}} - \underbrace{r_h \frac{O}{\kappa_{h_o} + O} B_{h1}}_{\text{R1}} - \underbrace{d_{h1} B_{h1}}_{\text{R2}} \\
\frac{\partial B_{h2}}{\partial t} &= \nabla \cdot (\sum_{j=1}^{4} D_{4j}(\mathbf{M}) \nabla M_j) + \underbrace{\mu_h \eta_d \frac{\kappa_{h_o}}{\kappa_{h_o} + O} \frac{A}{\kappa_a + A} \frac{N_2}{\kappa_{n2} + N_2} B_{h2}}_{\text{R5}} - \underbrace{d_{h2} B_{h2}}_{\text{R2}} \\
\frac{\partial N_1}{\partial t} &= \nabla \cdot (D_{n1}(M) \nabla N_1) - \underbrace{\frac{\mu_a M_\infty}{Y_n} \frac{O}{\kappa_{a_o} + O} \frac{N_1}{\kappa_{n1} + N_1} B_a}_{\text{R6}} \\
\frac{\partial N_2}{\partial t} &= \nabla \cdot (D_{n2}(M) \nabla N_2) + \underbrace{\frac{\mu_a M_\infty}{Y_n} \frac{O}{\kappa_{a_o} + O} \frac{N_1}{\kappa_{n1} + N_1} B_a}_{\text{R7}\cdots} \\
&\quad \underbrace{- \mu_h \eta_d M_\infty \frac{(1 - Y_h)}{2.58 Y_h} \frac{\kappa_{h_o}}{\kappa_{h_o} + O} \frac{A}{\kappa_a + A} \frac{N_2}{\kappa_{n2} + N_2} B_{h2}}_{\cdots\ \text{R7}} \\
\frac{\partial O}{\partial t} &= \nabla \cdot (D_o(M) \nabla O) - \underbrace{\frac{(4.57 - Y_n)}{Y_n} \mu_a M_\infty \frac{O}{\kappa_{a_o} + O} \frac{N_1}{\kappa_{n1} + N_1} B_a}_{\text{R8}\ \cdots} \\
&\quad \underbrace{- \frac{(1 - Y_h)}{Y_h} \mu_h M_\infty \frac{O}{\kappa_{h_o} + O} \frac{A}{\kappa_a + A} B_{h1} - r_a \frac{O}{\kappa_{a_o} + O} B_a - r_h \frac{O}{\kappa_{h_o} + O} B_{h1}}_{\cdots\ \text{R8}} \\
\frac{\partial A}{\partial t} &= \nabla \cdot (D_a(M) \nabla A) - \underbrace{\frac{\mu_h M_\infty}{Y_h} \frac{O}{\kappa_{h_o} + O} \frac{A}{\kappa_a + A} B_{h1}}_{\text{R9}\cdots} \\
&\quad \underbrace{- \frac{\mu_h \eta_d M_\infty}{Y_h} \frac{\kappa_{h_o}}{\kappa_{h_o} + O} \frac{A}{\kappa_a + A} \frac{N_2}{\kappa_{n2} + N_2} B_{h2}}_{\cdots\ \text{R9}}
\end{cases}
\tag{2.1}
$$

where M is the total biomass fraction, i.e. $M = I + B_a + B_{h1} + B_{h2}$ and $\mathbf{M} = (I, B_a, B_{h1}, B_{h2})$. Diffusion terms in the biomass equations that are responsible for spatial spreading of biofilm contain density dependent self- and cross-diffusion coefficients $D_{ij}(I, B_a, B_{h1}, B_{h2})$ $i, j \in \{1, 2, 3, 4\}$ $[m^2 d^{-1}]$ and gradient of biomass species denoted by $M_1 = I$, $M_2 = B_a$, $M_3 = B_{h1}$, and $M_4 = B_{h2}$. As explained in detail in previous studies [16, 23, 40], self- and cross diffusion coefficients are defined as:

$$\begin{cases} D_{ii}(I, B_a, B_{h1}, B_{h2}) = M_i \left(p(M)q'(M) - p'(M)q(M)\right) + p(M)q(M) \\ \\ D_{ij}(I, B_a, B_{h1}, B_{h2}) = M_i \left(p(M)q'(M) - p'(M)q(M)\right) \qquad \text{if } i \neq j \end{cases} \tag{2.2}$$

where $p(M)$ and $q(M)$ are defined as

$$p(M) = \frac{\delta}{5}(1 - M) \qquad\qquad q(M) = \left(\frac{M}{1 - M}\right)^4$$

The accent ($'$) in equation (2.2) represents derivative with respect to M and $\delta[m^2 d^{-1}]$ in functions $p(M)$ and $q(M)$ is the biomass motility coefficient which is positive but much smaller than the diffusion coefficients of dissolved substrates in liquid. The PDE system in (2.1) is a nonlinear reaction-diffusion model due to nonlinear effects represented by diffusion coefficients in biomass equations. The nonlinear effects are (i) porous medium degeneracy, i.e. $D_{ij}(M) \approx 0$ as total biomass, M, vanishes, (ii) a super-diffusion singularity as total biomass, M, approaches unity, and (iii) cross-diffusion. The power law degeneracy (i) guarantees propagation of the biofilm/liquid interface with finite speed and that the biofilm does not spread noticeably if there is locally space available for new biomass to accumulate. It is also responsible for the formation of a sharp interface $\Gamma(t)$ between biofilm and surrounding liquid. This indicates that initial data with compact support leads to solutions with compact support. The super-diffusion singularity (ii) ensures that the biomass fraction does not exceed unity as required physically and mathematically. The cross-diffusion terms with coefficient $D_{ij},\ i \neq j$ describe resistance to spatial spreading of one species due to the presence of other components, and subsequent mixing of species. The diffusion coefficients for substrates also depend on the total biomass fraction however in a non-critical manner. They are continuous functions bounded from above and below by two positive constants and are defined as $D_{n1,n2,o,a}(M) = D^0_{n1,n2,o,a}(1 + M(\rho_{(n1,n2,o,a)} - 1))$ where $D^0_{n1,n2,o,a}$ and $0 < \rho_{(n1,n2,o,a)} \leq 1$ are the diffusion coefficients in water and the biofilm/water ratio of diffusivities respectively. This reflects the fact that the substrate diffusion is slower in the biofilm than in the aqueous phase. Below is a summary of involved reaction terms:

- $R1$, $R2$: Formation of inert biomass through lysis and endogenous respiration. Endogenous respiration is described by Monod kinetics with maximum oxidation rate $r_{a,h}$ and half saturation constants κ_{a_o}, κ_{h_o}. The lysis is described as a first-order process with a constant rate $d_{a,h1,h2}$.
- $R3$: Growth of autotrophic bacteria (AB) in the presence of ammonium (as electron donor) and oxygen (as electron acceptor) described by dual Monod kinetics with μ_a as the maximum growth rate and κ_{a_o} and κ_{n1} as oxygen and ammonium half saturation constants respectively. In order to avoid making the problem more complicated than necessary, we assume oxygen half saturation constants in the growth and oxidation terms are the same. Furthermore, for simplicity and to avoid unnecessary complexity, we treat the nitrifiers as one species that oxidizes NH_4^+ directly to NO_3^-. Thus, the model does not consider the intermediate NO_2^- and ammonia oxidizers and nitrite oxidizers as distinct species [45, 46, 49].
- $R4$: Growth of Biological Oxygen Demand (BOD) degradation bacteria (heterotrophic bacteria (HB)) that consume oxygen as an electron acceptor and acetate as an electron donor. It is described by dual Monod kinetics with μ_h as the maximum growth rate and κ_{h_o} and κ_a as oxygen and acetate half saturation constants respectively.
- $R5$: Denitrification that involves growth of anaerobic heterotrophic bacteria (AHB) in the presence of acetate and nitrate (released as a side product of biological oxidation of ammonium) under anoxic condition. It is described by dual Monod kinetics with $\eta_d \mu_h$ as the maximum growth rate and κ_{h_o}, κ_a, and κ_{n2} as oxygen, acetate, and nitrate half saturation constants respectively.

- $R6$: Uptake of ammonium by autotrophic bacteria with yield coefficient Y_n.
- $R7$: production of nitrate as a result of biological oxidation of ammonium and its degradation by denitrifier bacteria with yield coefficients Y_n and Y_h.
- $R8$: Uptake of oxygen by autotrophic and aerobic heterotrophic bacteria.
- $R9$: Uptake of acetate by heterotrophic bacteria (aerobic and anaerobic).

3. Computational simulation

To solve the PDE system (2.1) numerically, appropriate boundary conditions must be defined. As the considered computational domain is a small part of a continuously repeating larger domain, we define the homogeneous Neumann condition for all dependent variables at the lateral boundaries, $x = 0, L$, to preserve the continuity [19]. To describe the involved counter-diffusion mechanism, we assume oxygen is provided through the membrane placed at the bottom boundary, $y = 0$, and organic and inorganic nitrogen sources are added through the top segment of the computational domain, $y = H$. Hence, a nonhomogeneous Robin condition is imposed for oxygen at $y = 0$ and for ammonium and acetate at $y = H$. The homogeneous Neumann condition is defined for nitrogen sources at the bottom boundary to reflect a hydrophobic membrane which does not permit these substances to diffuse through the membrane. We also assume that oxygen and nitrate are washed out through the top boundary nevertheless oxygen is not completely removed. Thus, nonhomogeneous and homogeneous Robin conditions are defined for oxygen and nitrate respectively at $y = H$. Moreover, it is assumed that there is no biomass flux at the top and bottom boundary, i.e. we specify homogeneous Neumann condition for biomass species at these boundaries. The boundary conditions for model (2.1) are as follows:

$$\begin{cases} \partial_n I = \partial_n B_a = \partial_n B_{h1} = \partial_n B_{h2} = 0 \ \text{ at } \partial\Omega \\ \partial_n O = \partial_n N_1 = \partial_n N_2 = \partial_n A = 0 \ \text{ at } x = 0,\ L \\ O + \lambda_o \frac{\partial O}{\partial n} = O_\infty \ \text{ at } y = 0 \\ O + \lambda_o \frac{\partial O}{\partial n} = 0.02 \ \text{ at } y = H \\ \partial_n N_1 = \partial_n N_2 = \partial_n A = 0 \ \text{ at } y = 0 \\ N_1 + \lambda_{n1} \frac{\partial N_1}{\partial n} = N_{1\infty} \ \text{ at } y = H \\ N_2 + \lambda_{n2} \frac{\partial N_2}{\partial n} = 0 \ \text{ at } y = H, \\ A + \lambda_a \frac{\partial A}{\partial n} = A_\infty \ \text{ at } y = H \end{cases} \tag{3.1}$$

where $\lambda_{(.)}[mm]$ is the concentration boundary layer thickness and describes the contribution of the convective contribution of external bulk flow to substrate supply [11]. Generally, the values of concentration boundary layer thickness are different at $y = 0$ and $y = H$. However, for simplicity, we assume that all substrates have the same concentration boundary layer thickness at the top and bottom boundaries, i.e. $\lambda_o = \lambda_{n1} = \lambda_{n2} = \lambda_a = \lambda$.

The primary objective of this study is investigating the role of inert biomass in SND performance under different environmental conditions and to address the question whether neglecting decay of biofilm causes any over or underestimation of substrate degradation and oxygen consumption. For this purpose,

depending on questions that will be addressed, different values of substrate bulk concentrations will be chosen in the range of $O_\infty = 5 \sim 25[g/m^3]$, $N_{1\infty} = 6 \sim 20[g/m^3]$, and $A_\infty = 3 \sim 12[g/m^3]$. The oxygen bulk concentration is the concentration of dissolved oxygen in the water adjacent to the membrane surface. Based on the oxygen Henry's law constant of $0.0228[bar/gm^{-3}]$ at 20°C [3], the selected range of O_∞ corresponds to an oxygen partial pressure in the range of 0.114 to 0.57 bar. This is in the range of the lower bound of air pressure on the gas side of the membrane (0.54 to 2.71 bar) when air with 21% oxygen content is used as the oxygen source. In fact this is reasonable because the air oxygen content decreases along the membrane length due to the oxygen consumption which makes the oxygen partial pressure on the gas side lower than that in the atmospheric air. The range of bulk concentrations for acetate and ammonium nitrogen are selected according to their effluent concentrations discharged from a continuous complete mix reactor when the reactor starts without significant nutrient availability. For the initial inoculation of the substratum, we consider two scenarios: homogeneous flat layer coverage and sparse inoculation. In both cases, the biofilm consists of autotrophic, aerobic and anaerobic heterotrophic bacteria. For comparability, the initial amount of biomass of all three types is the same in the two cases. Thickness of each layer in the flat layer inoculation is $20[\mu m]$ which makes the total initial thickness of the biofilm $60[\mu m]$. In the case of sparse inoculation, the substratum is covered by 6 semi-spherical colonies with radius $160[\mu m]$ centered at $x = 0.4$, $x = 1$, $x = 1.6$, $x = 2.4$, $x = 3$, and $x = 3.6[mm]$, c.f. Figure 2. Ammonium nitrogen and acetate are initially set to their bulk concentrations, and initial conditions for oxygen and nitrate nitrogen are half of the oxygen bulk concentration, i.e. $0.5O_\infty$ (for simplicity) and zero respectively.

For computational study of the effect of environmental conditions and formation of inert biomass on the nitrification/denitrification process and to investigate which pathway of decay contributes most to formation of inert biomass and to interpret the obtained results, we will provide two dimensional visualizations of simulations and define the following lumped output variables as quantities of interest:

- Total amount of biomass species:

$$U(t) = \int_\Omega U \; dxdy \quad U = I, B_a, B_{h1}, B_{h2} \tag{3.2}$$

- Total value of each production term in the equation for inert biomass per time:

$$P_i(t) = \int_\Omega P_i \; dxdy \tag{3.3}$$

where

$$\begin{cases} P_1 = f_d r_a \frac{O}{\kappa_{a_o}+O} B_a \\ P_2 = f_d r_h \frac{O}{\kappa_{h_o}+O} B_{h1} \\ P_3 = d_a B_a, \qquad P_4 = d_{h1} B_{h1}, \qquad P_5 = d_{h2} B_{h2} \end{cases} \tag{3.4}$$

- Total amount of degradation of substrates by biofilm:

$$\frac{1}{L} \int_\Omega R_{(n_1,n_2,o,a)} \; dxdy \; [g/m^2 d] \tag{3.5}$$

where

$$\begin{cases} R_{n_1} = \frac{\mu_a M_\infty}{Y_n} \frac{O}{\kappa_{a_o}+O} \frac{N_1}{\kappa_{n1}+N_1} B_a \\ R_{n_2} = \mu_h \eta_d M_\infty \frac{(1-Y_h)}{2.58 Y_h} \frac{\kappa_{h_o}}{\kappa_{h_o}+O} \frac{A}{\kappa_a+A} \frac{N_2}{\kappa_{n2}+N_2} B_{h2} \\ R_o = \frac{(4.57-Y_n)}{Y_n} \mu_a M_\infty \frac{O}{\kappa_{a_o}+O} \frac{N_1}{\kappa_{n1}+N_1} B_a + \frac{(1-Y_h)}{Y_h} \mu_h M_\infty \frac{O}{\kappa_{h_o}+O} \frac{A}{\kappa_a+A} B_{h1} \\ \quad + r_a \frac{O}{\kappa_{a_o}+O} B_a + r_h \frac{O}{\kappa_{h_o}+O} B_{h1} \\ R_a = \frac{\mu_h M_\infty}{Y_h} \frac{O}{\kappa_{h_o}+O} \frac{A}{\kappa_a+A} B_{h1} + \frac{\mu_h \eta_d M_\infty}{Y_h} \frac{\kappa_{h_o}}{\kappa_{h_o}+O} \frac{A}{\kappa_a+A} \frac{N_2}{\kappa_{n2}+N_2} B_{h2} \end{cases} \tag{3.6}$$

Simulations are terminated when 80% of the computational domain is occupied by the biofilm or when a pre-determined final time is reached.

For numerical solution of the PDE system (2.1), we first non-dimensionalize the system as: $\tilde{x} = x/H$ and $\tilde{t} = t\mu_h$ where H is the height of the computational domain and $\frac{1}{\mu_h}$ represents the characteristic time scale for growth of heterotrophic bacteria, $\tilde{N}_1 = \frac{N_1}{N_{1\infty}}$, $\tilde{N}_2 = \frac{N_2}{N_{1\infty}}$, $\tilde{O} = \frac{O}{O_\infty}$ and $\tilde{A} = \frac{A}{A_\infty}$. Note that the biomass volume fractions I, B_a, B_{h1}, and B_{h2} are already defined as dimensionless variables with respect to the maximum cell density M_∞. Then, we introduce a uniform grid of size $N \times M$ for the rectangular domain $[0, L/H] \times [0, 1]$ to discretize the dimensionless PDE model by a Finite Volume scheme. Due to the nonlinear diffusion effects (i), (ii), and (iii), the obtained ODE system is nonlinear and cannot be analyzed using standard arguments from the theory for ordinary differential equations, such as the Picard–Lindelöf theorem and the tangent condition cannot be readily applied to study the well-posedness of the ODE system [31]. Moreover, it is not a priori clear whether high order implicit standard numerical methods can be used for time integration of the resulting ODE system. Using regularization idea, it has been shown in previous studies [16, 17, 18] that the spatially discretised problem indeed satisfies a Lipschitz condition, i.e. has classical smooth solutions, indicating that singularity is never attained. Hence, time-adaptive error controlled integration techniques can be used to solve the resulting ODE model. In particular, we use the third order embedded Rosenbrock-Wanner method with 4 stages ROS3PRL [41] which requires in each time-step the solution of several sparse, large, non-symmetric linear systems, for which we use the stabilized bi-conjugate gradient method [17]. For efficient implementation of the code in terms of computational cost, OpenMP was used for the parallelization of selected computationally expensive tasks such as the linear solver and the formation of the Jacobian matrix within the Rosenbrock–Wanner method, and for the evaluation of nonlinear reaction terms. For a more detailed description of the numerical challenges and numerical method we refer to [16, 17].

Parameter values for numerical simulation and their description are summarized in Table 1.

4. Results

4.1. **Biofilm development and distribution of inert biomass.** The objectives of this section are to study the development of bacteria species within the biofilm and distribution of substrates for flat layer and sparse inoculation of the substratum (c.f. Figure 2). Results obtained at $N_{1\infty} = 12[gm^{-3}]$, $O_\infty = 15[gm^{-3}]$, and $A_\infty = 6[gm^{-3}]$ at times $t = 150$ and 300 are depicted in Figures 3-6. We observe that in the case of flat layer inoculation, inert biomass is formed mainly in the inner region of the biofilm at $t = 150$ due to decay of AB and HB while, as the biofilm grows (at $t = 300$), it is formed in the middle area closer to the biofilm/liquid interface. The biofilm is mostly composed of AB and AHB in this region indicating contribution of their decay to generation of inert biomass. Concentration of inert biomass reduces in a narrow region near the biofilm/liquid interface because of formation of less

TABLE 1. Model parameters for system (2.1) used for computer simulations

Parameter	Symbol	Value	Dimension	Source
Maximum specific growth rate for AB	μ_a	0.16	d^{-1}	[46]
Maximum specific growth rate for HB	μ_h	6	d^{-1}	[22]
Anoxic reduction factor for denitrification	η_d	0.8	–	[33]
Endogenous respiration rate for AB	r_a	0.0065	d^{-1}	[49]
Endogenous respiration rate for HB	r_h	0.25	d^{-1}	[49]
Non-biodegradable fraction of decayed biomass by endogenous respiration	f_d	0.2	–	[26]
Lysis rate for AB	d_a	0.05	d^{-1}	[27]
Lysis rate for HB, AHB	$d_{(h1,h2)}$	0.2	d^{-1}	[27]
Oxygen saturation constant for B_a	κ_{a_o}	0.5	gm^{-3}	[49]
Oxygen saturation constant for B_{h1}, B_{h2}	κ_{h_o}	2	gm^{-3}	[46]
Ammonium saturation constant	κ_{n1}	1	gm^{-3}	[46]
Nitrate saturation constant	κ_{n2}	0.5	gm^{-3}	[46]
Acetate saturation constant	κ_a	20	gm^{-3}	[46]
Yield of biomass produced from Ammonium	Y_n	0.24	–	[46]
Yield of biomass produced from Acetate	Y_h	0.66	–	[46]
Maximum cell density	M_∞	10^4	gm^{-3}	[49]
Diffusion coefficient for O in water	D_o^0	2×10^{-4}	m^2d^{-1}	[49]
Diffusion coefficient for N_1 in water	D_{n1}^0	1.7×10^{-4}	m^2d^{-1}	[49]
Diffusion coefficient for N_2 in water	D_{n2}^0	1.6×10^{-4}	m^2d^{-1}	[49]
Diffusion coefficient for A in water	D_a^0	1.5×10^{-4}	m^2d^{-1}	[46]
Biomass motility coefficient	δ	10^{-12}	m^2d^{-1}	[49]
Biofilm/water diffusivity ratio of O	ρ_o	1	–	[49]
Biofilm/water diffusivity ratio of N_1	ρ_{n1}	1	–	[49]
Biofilm/water diffusivity ratio of N_2	ρ_{n2}	1	–	[49]
Biofilm/water diffusivity ratio of A	ρ_a	0.25	–	[49]
Concentration boundary layer for oxygen	λ_o	0.4	mm	[21]
Concentration boundary layer for ammonium and acetate	$\lambda_{(n1,n2,a)}$	0.4	mm	*Assumed*
Oxygen bulk concentration	O_∞	15	gm^{-3}	[49]
Ammonium nitrogen bulk concentration	$N_{1\infty}$	12	gm^{-3}	*Assumed*
Acetate bulk concentration	A_∞	6	gm^{-3}	[49]
Length of the computational domain	L	4	mm	*Assumed*
Height of the computational domain	H	2	mm	*Assumed*

AB in this area. Snapshots of distribution of substrates are represented in Figure 4. The concentration of ammonium nitrogen decreases toward the bottom surface however it is not completely depleted in the region close to the membrane indicating that it is not a limiting factor for growth of AB. The concentration of oxygen provided through the membrane surface decreases within the biofilm as it grows such that an anoxic zone is formed in the outer surface at $t = 300$. These promote formation of AB and production of N_2 within the biofilm and formation of AHB in the region close to the biofilm/liquid interface at $t = 300$. At $t = 150$, HB is formed in the outer surface where the concentration of acetate

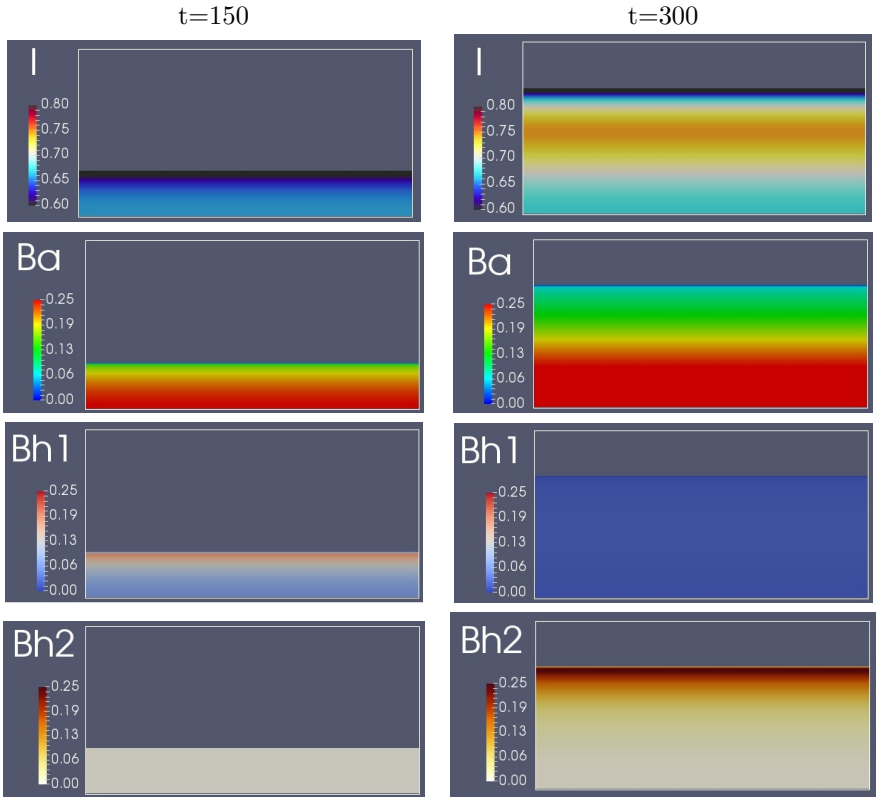

FIGURE 3. Snapshots of biofilm development for the flat layer coverage at $t = 150$ and $t = 300$. The bulk concentrations of substrates are set at $N_{1\infty} = 12[gm^{-3}]$, $O_\infty = 15[gm^{-3}]$, and $A_\infty = 6[gm^{-3}]$. Note that the color coding scale for inert biomass is different for better visualization of concentration gradient.

is higher and oxygen is not limited while oxygen depletion and consumption of acetate by AHB inhibit formation of HB at $t = 300$. It has been shown in [19, 20] that initial arrangement of individual colonies changes the internal structure of the biofilm and spatial distribution of substrates nevertheless its effect on nitrification and denitrification is not considerable. To investigate whether formation of inert biomass is affected by initial inoculation of the substratum, we study development of biofilm with initial sparse inoculation (that needs a 2D modeling approach to be described) and plot snapshots of biofilm development and substrate distribution in Figures 5-6. The results obtained at $t = 150$ show that individual colonies that are closer together merge into single colonies at $t < 150$ and then form a thick biofilm at $t = 300$. At $t = 150$, the inert biomass is mostly formed in the right side of the colonies where more HB and small amount of AHB are formed. Note that AB that occupy the right side of the colonies generate lower amounts of inert biomass in this region due to their lower respiration rate. As the biofilm grows, the inert biomass occupies the whole biofilm with lower concentration in the inner layers of the biofilm and higher concentration in the outer surface. The specific initial arrangement used in this study yields formation of AB mostly in the left corner of colonies that consequently results in the higher concentration of N_2 in this area, production of HB and lower concentration of acetate in the middle, and formation of AHB in the small area of the right corner of the colonies at $t = 150$. Nevertheless, as the biofilm grows and colonies merge, AB occupy the whole biofilm heterogeneously

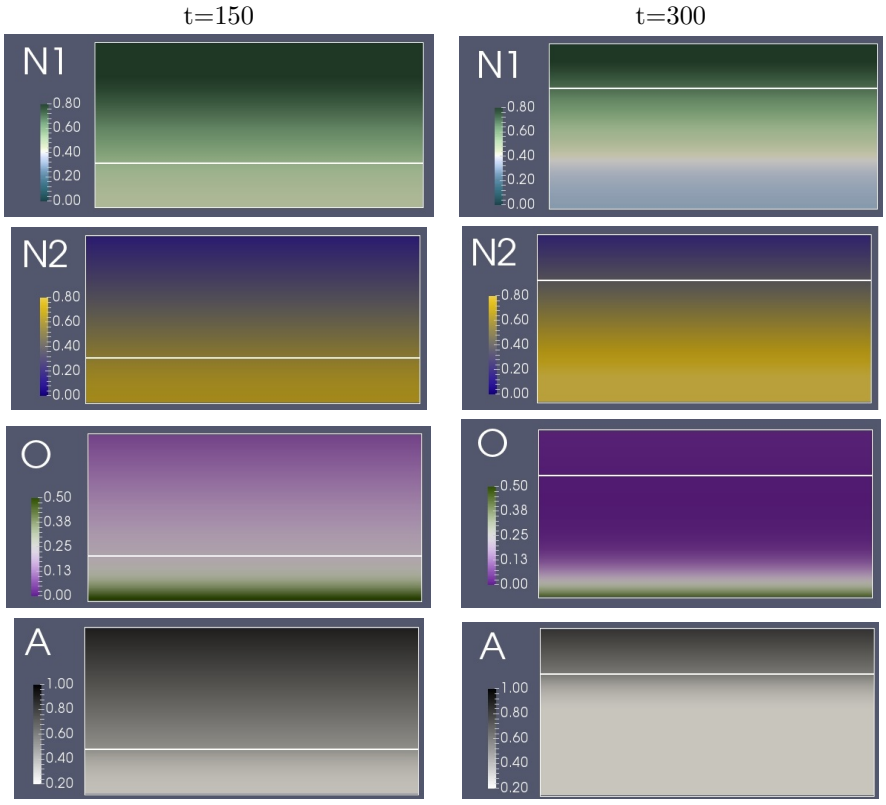

FIGURE 4. Snapshots of substrate distribution for the flat layer coverage at $t = 150$ and $t = 300$. The bulk concentrations of substrates are set at $N_{1\infty} = 12[gm^{-3}]$, $O_\infty = 15[gm^{-3}]$, and $A_\infty = 6[gm^{-3}]$. Note that the color coding scales are different for better visualization of concentration gradient. The solid white line shows the biofilm/liquid interface.

except a narrow region closer to the biofilm/liquid interface while HB and AHB are formed in the outer surface. Moreover, at $t = 300$ concentration gradient of substrates decreases across the biofilm and they behave more homogeneously, similar to the flat layer scenario.

Results in Figures 3-6 indicate that the effect of initial inoculation on the internal structure of the biofilm is profound at the early stage of biofilm growth and becomes less significant in a well established biofilm. Nevertheless, as the results in Figure 7 show, initial inoculation does not change the total amount of produced inert biomass significantly. Hence since this study focuses on the importance of including inert biomass in modeling the SND performance of an MABR and since both cases of initial inoculation are relevant from a biofilm reactor performance perspective, for further study of SND and generation of inert biomass under different environmental conditions we use the homogeneous case to reduce computational cost. Note that the cases studied in this section are demonstrative examples and other scenarios are possible. We refer to [19] for other possible configurations.

According to the results obtained in this section and comparing them with the results in [20], neglecting the role of inert biomass as a volume occupying species in modeling the performance of MABRs gives an inaccurate description of biofilm structure and consequently the SND performance.

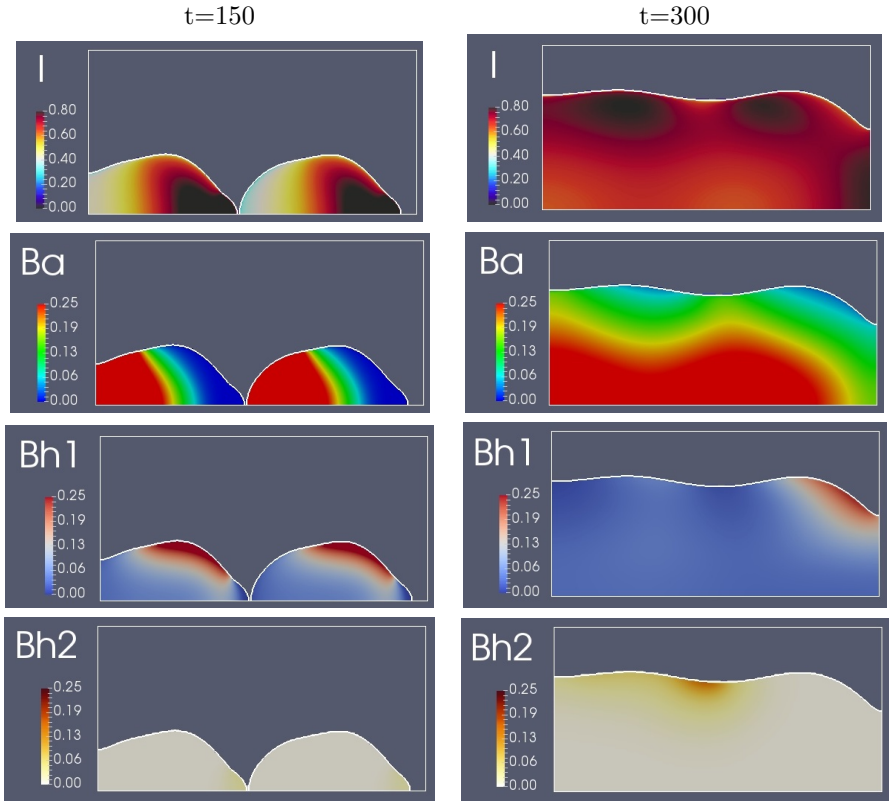

FIGURE 5. Snapshots of biofilm development for the sparse inoculation at $t = 150$ and $t = 300$. The bulk concentrations of substrates are set at $N_{1\infty} = 12[gm^{-3}]$, $O_\infty = 15[gm^{-3}]$, and $A_\infty = 6[gm^{-3}]$. Note that the color coding scale for inert biomass is different for better visualization of concentration gradient.

4.2. **Contribution of endogenous respiration and cell lysis to generation of inert biomass.** In MABRs inert biomass is accumulated within the biofilm but it is not easy to determine the mechanism of its formation experimentally. Nevertheless, we can discover the main source for production of inert biomass computationally under different environmental conditions. For this purpose, we compute total value of each production term of inert biomass as defined in (3.5) at $N_{1\infty} = 12[gm^{-3}]$, $O_\infty = 15[gm^{-3}]$, $A_\infty = 6[gm^{-3}]$ as a standard condition and at lower concentrations of each substrate to investigate how it changes with respect to bulk concentrations of substrates. Results obtained for four considered cases (Figure 8) show that respiration of AB makes the minimum contribution to inert biomass, due to its slower growth, followed by respiration of HB. The main inert biomass generators are lysis of bacteria species. However, contribution of each species varies depending on substrate concentrations and biofilm thickness. Under the standard condition used in this study, lysis of AB increases with time monotonically while lysis of HB increases until $t \approx 219$ (biofilm thickness $\approx 0.84[mm]$) albeit in a non-monotonic behavior with some oscillations in between and then declines sharply due to inhibition of HB growth in thick biofilm. Respiration of HB initially increases until $t \approx 100$ and then decreases and ultimately diminishes at the end of the simulation. Contribution of lysis of AHB is negligible at the beginning, but it starts increasing at $t \approx 230$ due to formation of AHB and it becomes dominant for $t > 300$. These results show that lysis of biomass species with higher abundance has major impact on the

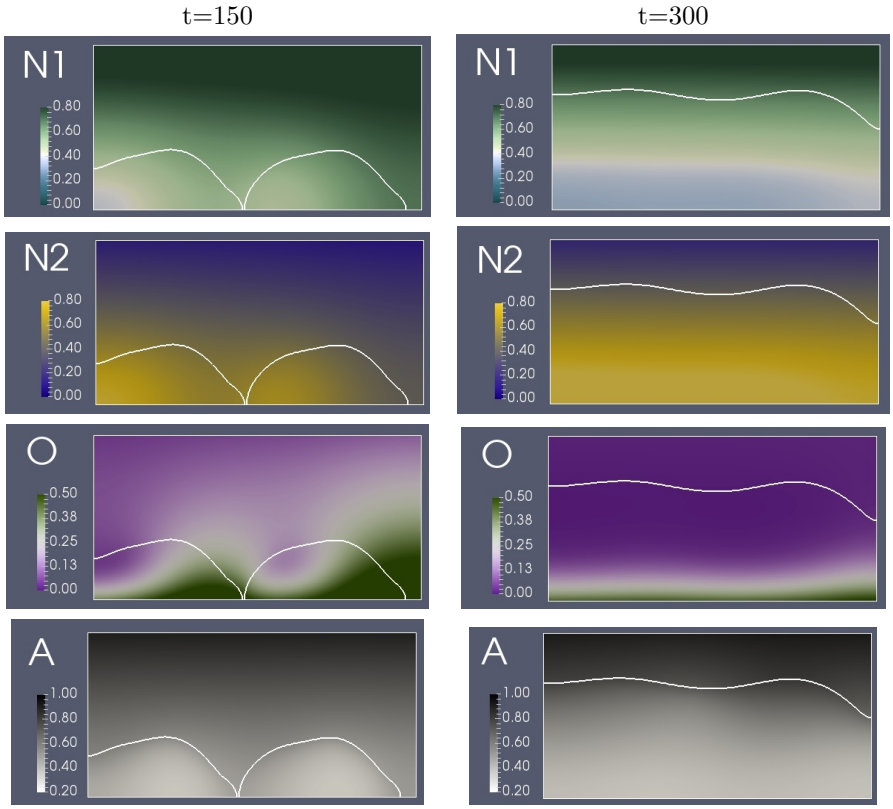

FIGURE 6. Snapshots of substrate distribution for the sparse inoculation at $t = 150$ and $t = 300$. The bulk concentrations of substrates are set at $N_{1\infty} = 12[gm^{-3}]$, $O_\infty = 15[gm^{-3}]$, and $A_\infty = 6[gm^{-3}]$. Note that the color coding scales are different for better visualization of concentration gradient. The solid white line shows the biofilm/liquid interface.

accumulation of inert biomass and residual of endogenous respiration does not play a key role. Figure 8b shows the results for $A_\infty = 3[gm^{-3}]$ while the bulk concentration of ammonium nitrogen and oxygen are not changed. Decreasing the bulk concentration of acetate from $6[gm^{-3}]$ to $3[gm^{-3}]$ reduces the production of heterotrophic bacteria which consequently makes lysis of autotrophic bacteria the major contributor after $t > 100$ followed by lysis of AHB at $t > 340$ (Figure 8b). Decreasing the ammonium nitrogen bulk concentration from $12[gm^{-3}]$ to $6[gm^{-3}]$ at $O_\infty = 15[gm^{-3}]$ and $A_\infty = 6[gm^{-3}]$ decreases the growth of AB and makes lysis of HB the main contributor to inert biomass production during the whole simulation period (Figure 8c). Moreover, since slower growth of AB leaves more oxygen for growth of HB, the effect of its endogenous respiration becomes more significant compare to the results obtained in other cases however it is not a determining factor. Reducing the bulk concentration of oxygen to $O_\infty = 5[gm^{-3}]$ makes the growth condition more suitable for anaerobic heterotrophic bacteria, the lag time for its formation shorter, and respiration pathways less dominant, such that lysis of AHB becomes dominant inert biomass generator after $t > \approx 200$ (Figure 8d).

4.3. **Substrate distribution within the biofilm.** Snapshots of distribution of substrates along a vertical line at the middle of the domain ($= 2[mm]$) for flat layer inoculation of the substratum at times $t = 60, 150, 210$ for the cases with and without decay are depicted in Figure 9. The results are obtained

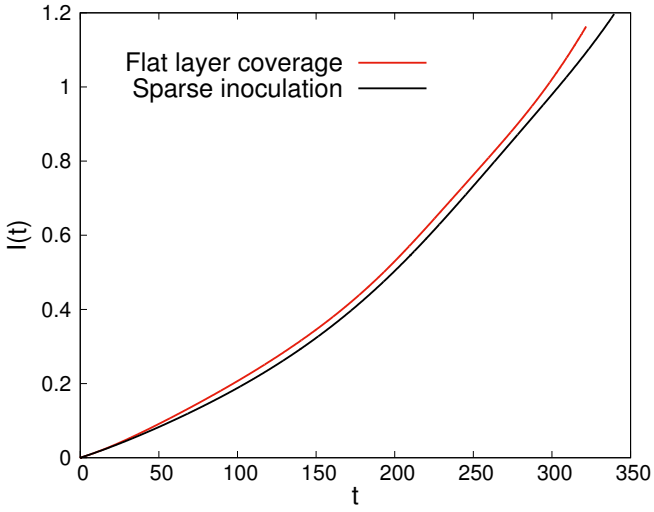

FIGURE 7. Total amount of generated inert biomass for flat layer and sparse inoculation. The bulk concentrations of substrates are set at $N_{1\infty} = 12[gm^{-3}]$, $O_\infty = 15[gm^{-3}]$, and $A_\infty = 6[gm^{-3}]$.

at $N_{1\infty} = 12[gm^{-3}]$, $O_\infty = 15[gm^{-3}]$, and $A_\infty = 6[gm^{-3}]$. The oxygen profiles at different times with and without including inert biomass show the maximum oxygen concentration at the membrane surface ($y = 0$) and the minimum at the top boundary. If inert biomass is not included anoxic zone is formed at $t = 150$ and oxygen is depleted in the region $y > 0.8[mm]$, while with taking into account the inert biomass, anoxic zone is not formed during the whole simulation period indicating the lower rate of oxygen consumption by the biofilm containing inert biomass. The simulation also illustrates that the oxygen concentration gradient across the biofilm is slightly steeper for the case with inert biomass, reflecting that the oxygen transfer resistance increases within the biofilm when inert biomass is included. Figure 9 also shows the impact of including the inert biomass on acetate distribution. Acetate is added to the domain through the top boundary, and it is consumed within the biofilm by HB and AHB. Hence, its concentration decreases in biofilm toward the membrane surface. The simulation shows a significant difference in spatial distribution of acetate for the cases with and without inert biomass. Without inert biomass acetate is completely depleted in the region close to the membrane surface for $t > 150$, while in the case with inert biomass it exists everywhere in the domain at all three times indicating the overestimation of density of heterotrophs in the case with no inert biomass. The simulation results in Figure 9 reveal that there is a great amount of ammonium in the domain at all times however its concentration decreases toward the membrane surface. Due to formation of more AB in the case without inert biomass, the concentration of ammonium nitrogen is lower within the biofilm making the ammonium nitrogen concentration gradient between biofilm and liquid steeper in this case. The concentration of nitrate nitrogen decreases from the membrane surface (where more AB are formed) to the top boundary (where more AHB are produced). Without including inert biomass, more nitrate is produced because of formation of more AB and more nitrate is also consumed due to formation of more anaerobic heterotrophs.

4.4. **Effect of substrate concentrations on formation of inert biomass.** Production of inert biomass in biofilms can be affected by the concentration and spatial distribution of oxygen, ammonium nitrogen, and acetate as they control biofilm growth and structure of microbial communities. To study

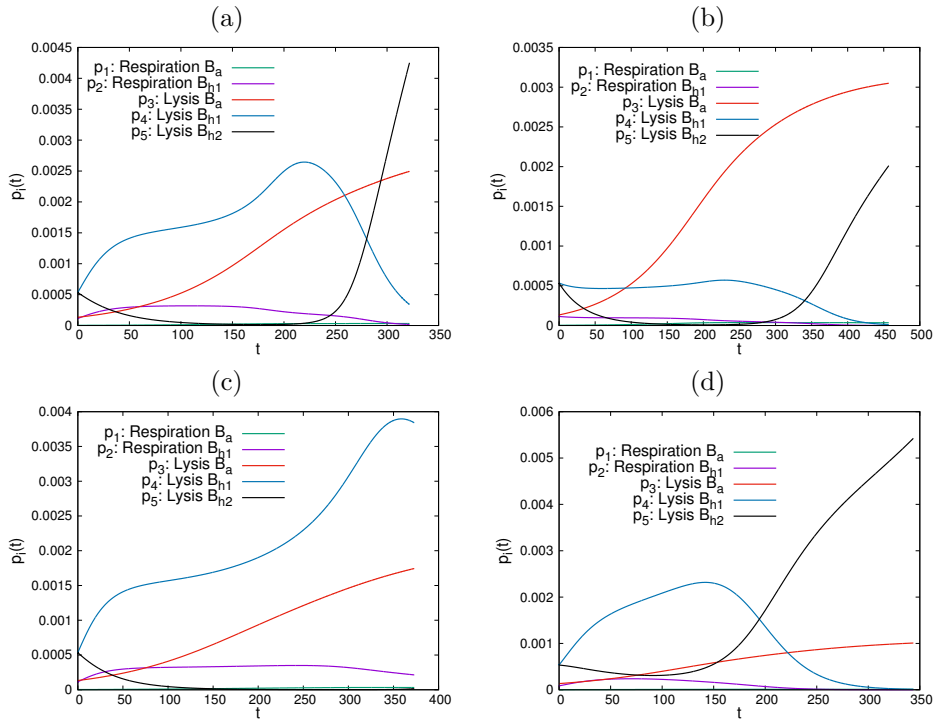

FIGURE 8. Dynamics of decay pathways for each bacteria species. (a): A standard condition with $N_{1\infty} = 12[gm^{-3}]$, $O_\infty = 15[gm^{-3}]$, $A_\infty = 6[gm^{-3}]$; (b) At lower acetate concentration $A_\infty = 3[gm^{-3}]$, (c) At lower ammonium nitrogen concentration $N_{1\infty} = 6[gm^{-3}]$, (d) At lower oxygen concentration $O_\infty = 5[gm^{-3}]$.

the effects of bulk concentrations of substrates on the accumulation of inert biomass is the objective in this section. For this purpose, we change the bulk concentration of substrates and record the total amount of inert biomass for each case. Results are depicted in Figure 10. Figure 10a shows the effect of $O_\infty[gm^{-3}]$ on production of inert biomass under the condition of $N_{1\infty} = 12[gm^{-3}]$ and $A_\infty = 6[gm^{-3}]$. Increasing O_∞ doesn't make significant difference in formation of inert biomass, indicating the balance between production of inert and active biomass with increasing the bulk oxygen concentration. However, the lowest concentration of bulk oxygen produces slightly larger amount of inert biomass which, as shown in Figure 8, is mostly related to the lysis of HB until $t \approx 200$ and lysis of AHB after that. Figure 10b shows the impact of $N_{1\infty}[gm^{-3}]$ on the formation of inert biomass at $O_\infty = 15[gm^{-3}]$ and $A_\infty = 6[gm^{-3}]$. Initially, until $t \approx 150$ (biofilm thickness $0.46[mm]$), varying the bulk concentration of ammonium nitrogen shows insignificant effect on $I(t)$. As the biofilm grows, the results diverge such that more inert biomass is produced at higher bulk concentration of ammonium nitrogen. The ammonium nitrogen concentration affects growth of autotrophic bacteria and consequently available oxygen for production of heterotrophs, formation of anoxic zone and growth of AHB. At higher bulk concentrations of ammonium nitrogen that promote formation of AB and AHB, inert biomass is formed mostly because of lysis of these species. Figure 10c shows the impact of $A_\infty[gm^{-3}]$ on $I(t)$ at $N_{1\infty} = 12[gm^{-3}]$ and $O_\infty = 15[gm^{-3}]$. By increasing A_∞ the amount of generated inert biomass increases nevertheless it reaches ≈ 1.18 at the end of the simulation for all cases. Moreover, the required time for biofilm to occupy 80% of the computational domain becomes shorter due to formation of more heterotrophic

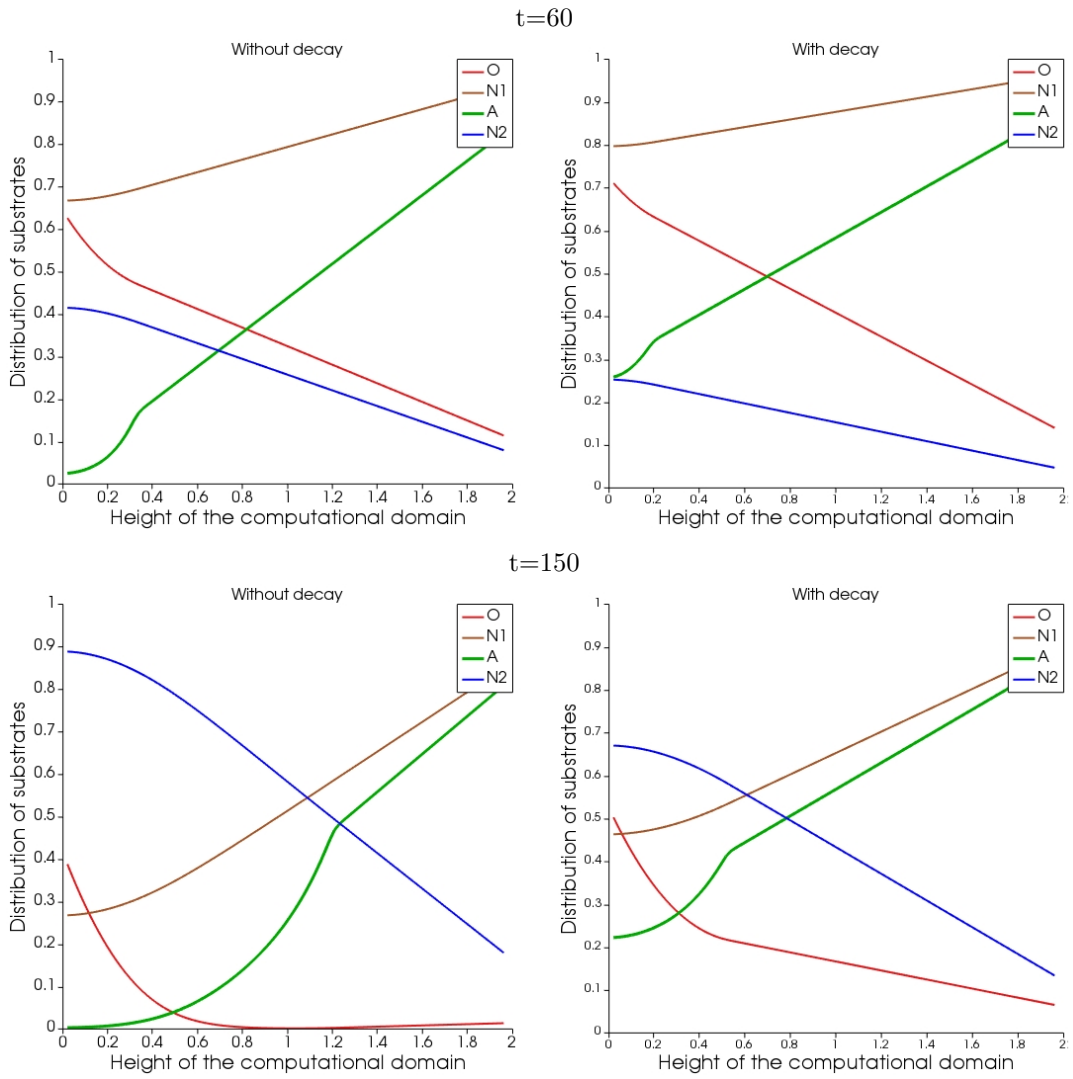

bacteria that grow fast. The main contributors to accumulation of inert biomass at high concentrations of acetate are endogenous respiration of HB and lysis of AB at the beginning and lysis of AB and AHB when the biofilm is well established, c.f. Figure 8.

The simulation results represented in sections 4.1-4.4 suggest that it is necessary to consider the presence of inert biomass in MABR modeling for more accurate description of its performance. In the subsequent sections 4.5-4.7, we will analyze the effect of bulk concentrations of oxygen, ammonium nitrogen, and acetate on nitrification, denitrification, and study consumption of oxygen and nitrogen sources.

4.5. **Factors affecting nitrification.** Figures 11a-f show the results of impact of substrate bulk concentrations $O_\infty[gm^{-3}]$, $N_{1\infty}[gm^{-3}]$, and $A_\infty[gm^{-3}]$ on the formation of AB and nitrification. As the results in Figure 11a show, $B_a(t)$ increases for all values of $O_\infty[gm^{-3}]$ and reaches $\approx$ 0.12, 0.22, 0.3, 0.39 at $t \approx 318$ (end of the simulation for $O_\infty = 25[gm^{-3}]$) for $O_\infty = 5$, 10, 15, $25[gm^{-3}]$ respectively.

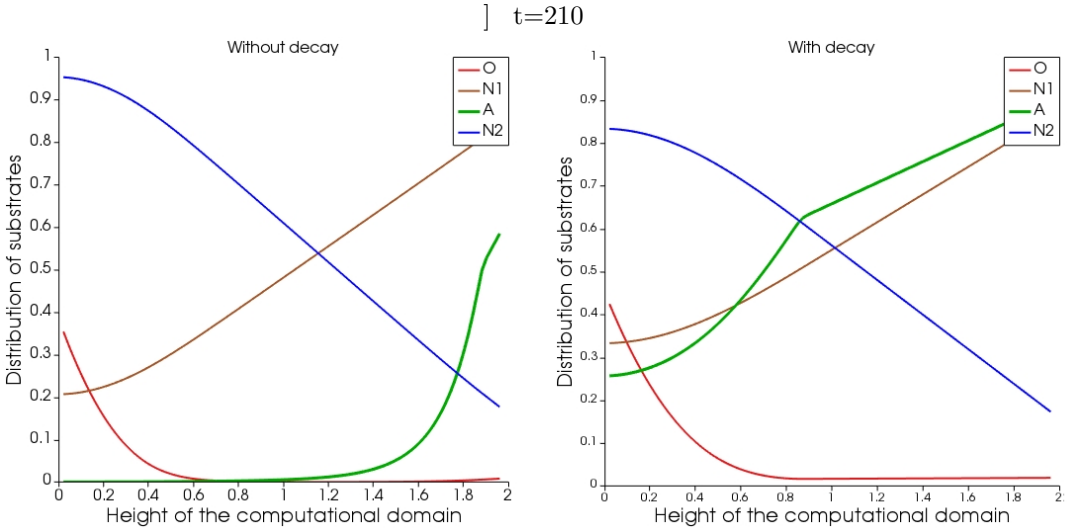

FIGURE 9. Snapshots of distribution of substrates within the computational domain along the line $x = 2[mm]$ (middle of the domain) at $t = 60$, $t = 150$, and $t = 210$ for the cases with and without decay. The bulk concentrations of substrates are set at $N_{1\infty} = 12[gm^{-3}]$, $O_\infty = 15[gm^{-3}]$, and $A_\infty = 6[gm^{-3}]$.

However, it becomes gradually stagnant at lower concentrations of oxygen. Figure 11b shows that increasing $O_\infty[gm^{-3}]$ improves the nitrification rate due to the formation of more autotrophic bacteria at higher concentrations of bulk oxygen. The nitrification rates obtained for different concentrations of bulk oxygen initially increase and then gradually reach plateaus particularly at lower concentrations with values increasing from $\approx 0.3[gm^{-2}d^{-1}]$ at $O_\infty = 5[gm^{-3}]$ to $\approx 1.1[gm^{-2}d^{-1}]$ at $O_\infty = 25[gm^{-3}]$ at $t \approx 318$, c.f. Figure 11b. According to the results in Figure 11a-b, increasing the bulk oxygen concentration increases the amount of AB resulting in an increase in the nitrification rates however the improvement occurs when biofilm thickness exceeds a threshold. Figures 11c-d show the effect of bulk concentration of ammonium nitrogen on formation of AB and nitrification rate. The simulation results show that more autotrophic bacteria are present inside the biofilm at higher concentrations of ammonium nitrogen and $B_a(t)$ increases from ≈ 0.18 to ≈ 0.32 at $t \approx 305$ (end of the simulation for $N_{1\infty} = 20[gm^{-3}]$) with increasing $N_{1\infty}[gm^{-3}]$ from $6[gm^{-3}]$ to $20[gm^{-3}]$ at $O_\infty = 15[gm^{-3}]$ and $A_\infty = 6[gm^{-3}]$. Increasing the production of autotrophic bacteria improves the nitrification rates such that it reaches from $0.55[gm^{-2}d^{-1}]$ for $N_{1\infty} = 6[gm^{-3}]$ to $\approx 0.87[gm^{-2}d^{-1}]$ for $N_{1\infty} = 20[gm^{-3}]$ at $t \approx 305$, c.f. Figure 11d. Figures 11e-f show the impact of the bulk acetate concentrations on formation of AB and nitrification rates. The simulation results show that formation of autotrophic bacteria is not notably sensitive to changes in $A_\infty[gm^{-3}]$ from 3 to $12[gm^{-3}]$ at $O_\infty = 15[gm^{-3}]$ and $N_{1\infty} = 12[gm^{-3}]$. However, with the increase in biofilm thickness, a higher nitrification rate can be achieved at lower bulk acetate concentrations. For the conditions used in this study ($O_\infty = 15[gm^{-3}]$ and $N_{1\infty} = 12[gm^{-3}]$), changing the bulk acetate concentration does not initially change the nitrification rate but later on (when the biofilm reaches appropriate thickness) it slightly increases by decreasing $A_\infty[gm^{-3}]$ due to the formation of more autotrophic bacteria at lower acetate concentrations. The nitrification rate increases from $\approx 0.63[gm^{-2}d^{-1}]$ to $\approx 0.78[gm^{-2}d^{-1}]$ at $t \approx 186$ (end of the simulation for $A_\infty = 12[gm^{-3}]$) as $A_\infty[gm^{-3}]$ decreases from $12[gm^{-3}]$ to $3[gm^{-3}]$. Thus, the simulation results reveal that the nitrification performance of MABR is mainly affected by the oxygen supply, bulk ammonia concentration, and

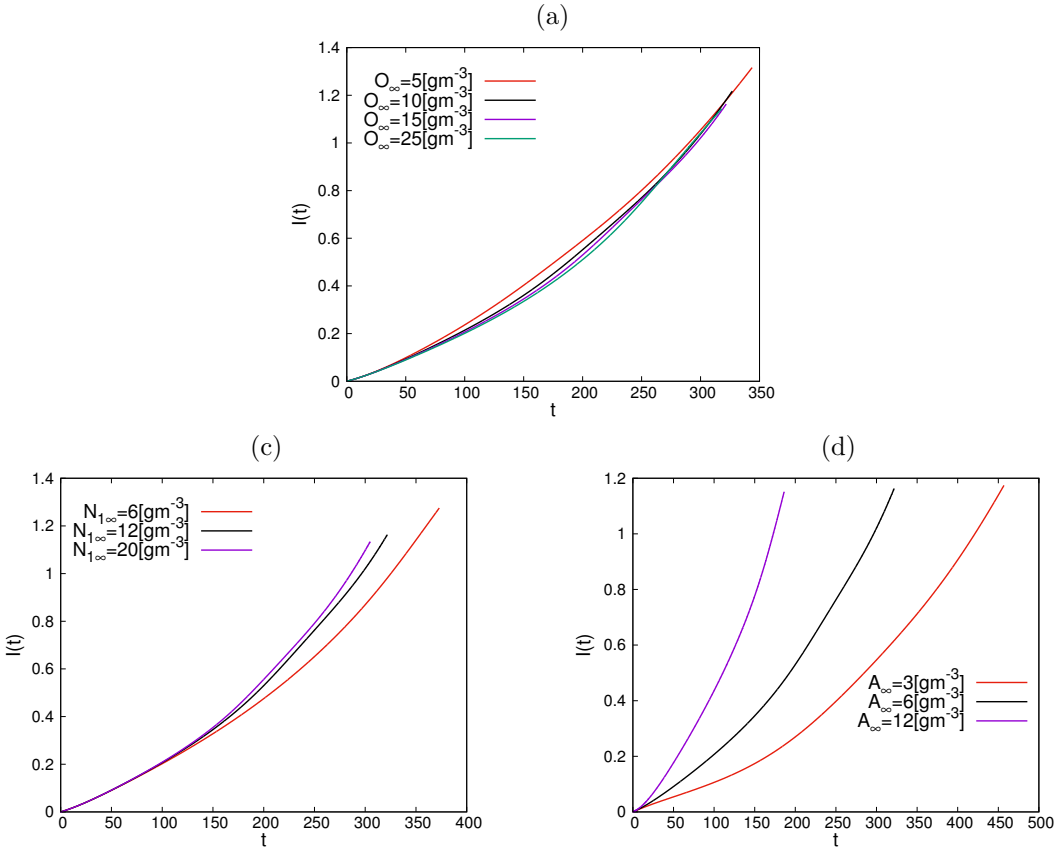

FIGURE 10. Time evolution of total amount of inert biomass for different values of substrate bulk concentrations.

biofilm thickness. The impact of organic carbon on the nitrification performance of MABR is limited and mainly because of its effect on the biofilm thickness and oxygen distribution after formation of HB. To show how including inert biomass in modeling the SND process changes the results, we repeat the simulations without inert biomass and calculate total amount of autotrophic bacteria and degradation of ammonium at $N_{1\infty} = 12[gm^{-3}]$, $N_{1\infty} = 6[gm^{-3}]$, and $O_\infty = 15[gm^{-3}]$. The results are shown by dashed lines in Figure 11. Comparing the results for $B_a(t)$ and nitrification rates for the cases with and without inert biomass, obtained under the same conditions, show that inclusion of inert biomass results in lower values of B_a and nitrification rates. It also takes longer for $B_a(t)$ and nitrification rate to reach their stable values if inert biomass is included. These results indicate that it is necessary to consider the inert biomass component of biofilm for more accurate simulation of MABR nitrification performance.

4.6. **Factors affecting denitrification.** Figures 12a-f show the results of the effect of O_∞, $N_{1\infty}$, and A_∞ on the formation of AHB and denitrification rates. Results obtained for $B_{h2}(t)$ and denitrification rates at different values of $O_\infty[gm^{-3}]$ for $N_{1\infty} = 12[gm^{-3}]$, $A_\infty = 6[gm^{-3}]$ are represented in Figures 12a and b. As shown in these figures, $B_{h2}(t)$ starts increasing at $t \approx 140$ and reaches ≈ 0.16 at the end of the simulation for $O_\infty = 5[gm^{-3}]$. Increasing the oxygen bulk concentration delays the enrichment of B_{h2} and reduces the amount of AHB in the biofilm because of the production of more HB and

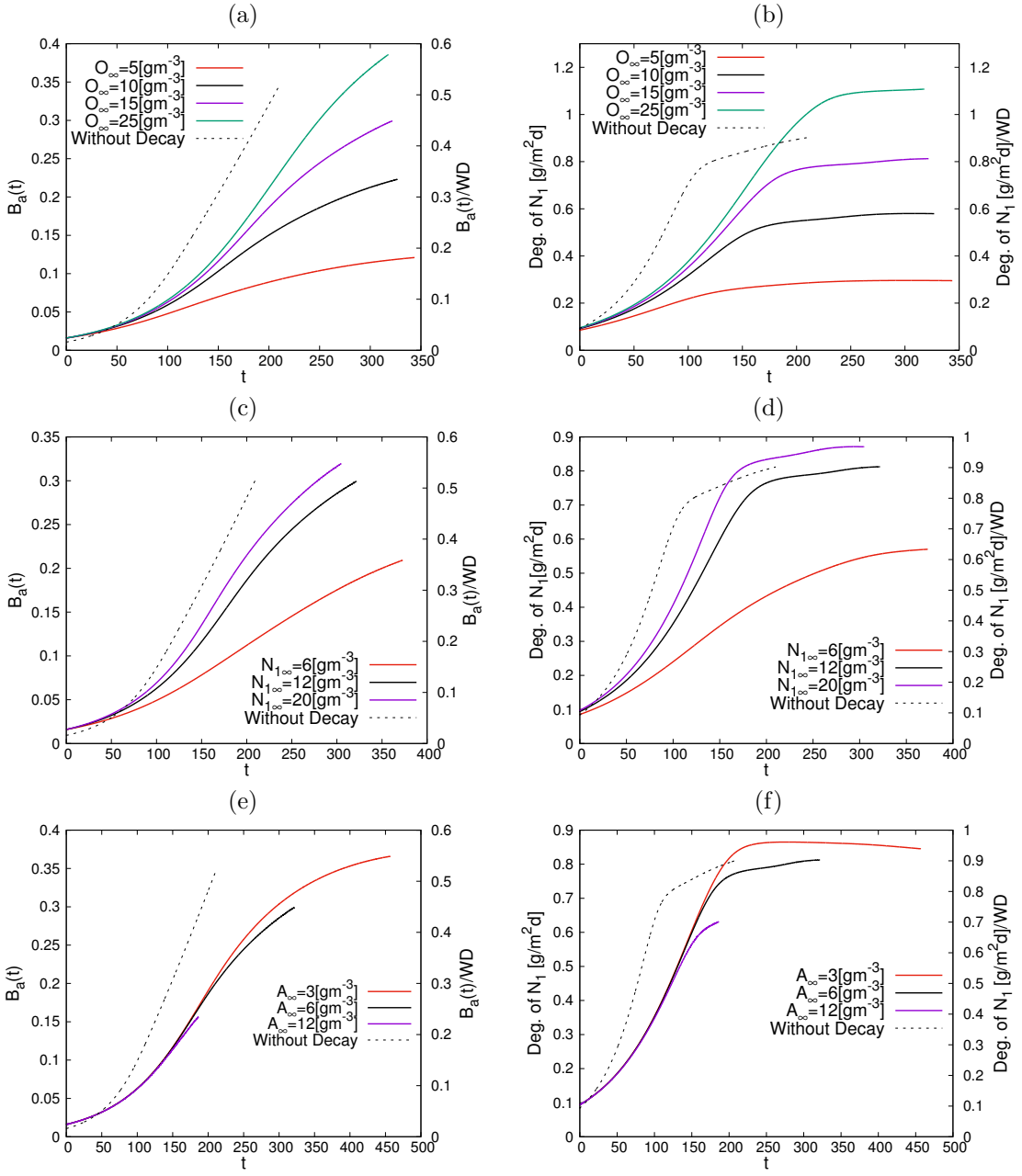

FIGURE 11. Time evolution of total amount of autotrophic biomass (B_a) and degradation of ammonium for different values of dissolved substrates. Dashed line shows the results at standard condition ($O_\infty = 15[gm^{-3}]$, $N_{1\infty} = 12[gm^{-3}]$, $A_\infty = 6[gm^{-3}]$) on the right axis for the case without decay terms.

inhibition of formation of anoxic zone. At the highest bulk concentration of oxygen ($O_\infty = 25[gm^{-3}]$) AHB is not produced significantly due to oxygen abundance that inhibits formation of anoxic zone before termination of the simulation. However, although increasing $O_\infty[gm^{-3}]$ delays the growth of AHB, they grow fast once the anoxic zone is established because of the access to acetate near the

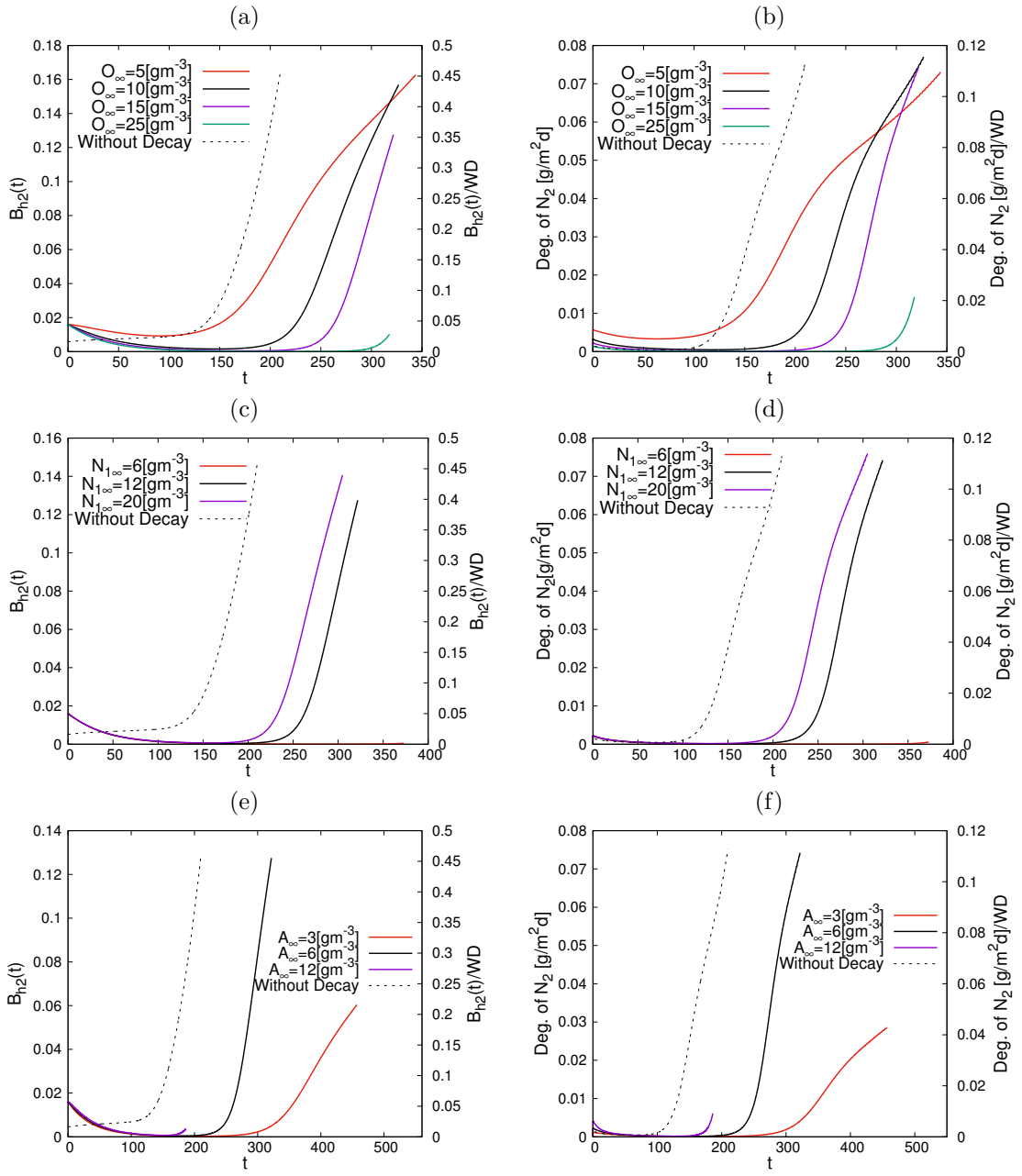

FIGURE 12. Time evolution of total amount of anaerobic heterotrophic bacteria biomass (B_{h2}) and degradation of nitrate for different values of dissolved substrates. Dashed line shows the results at standard condition ($O_\infty = 15[gm^{-3}]$, $N_{1\infty} = 12[gm^{-3}]$, $A_\infty = 6[gm^{-3}]$) on the right axis for the case without decay terms.

outer surface of the biofilm. Thus, overall, denitrification has a shorter lag time and a higher rate at lower concentrations of oxygen. Total amount of B_{h2} and denitrification rate obtained for ammonium nitrogen concentrations in the range of 6 to 20$[gm^{-3}]$ at $O_\infty = 15[gm^{-3}]$ and $A_\infty = 6[gm^{-3}]$ are shown in Figures 12c-d. Increasing $N_{1\infty}[gm^{-3}]$ makes the lag time for the formation of anoxic zone shorter,

facilitating growth of AHB. For example, by increasing the bulk ammonium nitrogen concentration from 12 to 20$[gm^{-3}]$, the lag time for growth of AHB reduces from ≈ 230 to ≈ 200 and the denitrification rate at $t \approx 305$ increases from 0.06 to 0.07$[gm^{-2}d^{-1}]$ (Figures 12c-d). At $N_{1\infty} = 6[gm^{-3}]$, AHB is not formed prior to the termination of the simulation, resulting in no denitrification in this case during the simulation period. Figures 12e-f show the effect of acetate concentrations ($A_\infty = 3,\ 6,\ 12[gm^{-3}]$) on B_{h2} and denitrification rate at $O_\infty = 15[gm^{-3}]$ and $N_{1\infty} = 12[gm^{-3}]$. AHB is not formed at $A_\infty = 12[gm^{-3}]$ and the small amount of AHB that is initially available vanishes because of the fast occupancy of the biofilm by HB under this condition that also results in an earlier termination of the simulation. Decreasing A_∞ to $6[gm^{-3}]$ produces less HB and $B_{h2}(t)$ starts to increase at $t \approx 205$ and reaches ≈ 0.13 at the end of the simulation ($t \approx 322$) with a denitrification rate $\approx 0.075[gm^{-2}d^{-1}]$ achieved at this time. However, further decrease in A_∞ to $3[gm^{-3}]$ results in production of less HB which leaves more oxygen for the growth of AB. Slow growth rate of AB, delays establishment of anoxic zone and formation of AHB. Under this condition, $B_{h2}(t)$ starts to increase at $t \approx 300$ and reaches 0.06 at the end of the simulation with a denitrification rate $\approx 0.03[gm^{-2}d^{-1}]$ achieved at this time. This implies that when the biofilm growth is limited by carbon sources, denitrification can only be established with reduced oxygen concentration. Hence, according to the results obtained in this section, very low or very high concentration of acetate can inhibit denitrification. At very low concentrations, AHB is not produced considerably due to acetate shortage, while at high acetate concentrations AHB will be arrested by the overgrowth of HB. However, optimization of oxygen supply can help to establish denitrification under these conditions.

To show how taking inert biomass into account in modeling the SND process affects the results, we repeat the simulations without inert biomass at $N_{1\infty} = 12[gm^{-3}]$, $A_\infty = 6[gm^{-3}]$, and $O_{1\infty} = 15[gm^{-3}]$. Results are shown by dashed lines in Figure 12. Comparing the degradation rates achieved at the same environmental conditions for the cases with and without decay shows that presence of inert biomass significantly delays denitrification and reduces its rates. Thus, inclusion of biomass decay is necessary to simulate MABR denitrification performance more accurately.

4.7. **Consumption of oxygen and nitrogen sources.** Key factors in determining the efficiency of SND performance are consumption of oxygen and substrate degradation by biofilm. Range of biofilm thickness that yields minimum oxygen consumption and maximum removal of nitrogenous sources can be considered an optimum thickness at which an efficient SND is achieved. To see if we can find a required or an optimum biofilm thickness for effective SND, we compute the ratio of consumption of O to degradation of N_1 (OC/DN1) and degradation of N_2 to degradation of A (DN2/DA) within the biofilm for various bulk concentrations of substrates. For easier physical interpretation and to find a required biofilm thickness that results in effective SND performance, we calculate the biofilm thickness as time proceeds and record the ratios at each value of the biofilm thickness. Simulation in all cases is terminated when 80% of the computational domain is occupied by the biofilm. Results obtained for various O_∞, $N_{1\infty} = 12[gm^{-3}]$ and $A_\infty = 6[gm^{-3}]$ show that after the initial growth of biofilm, OC/DN1 slightly increases and then decreases as biofilm grows. Initial increment of the ratio is due to the growth of HB which consumes oxygen at higher rate compare to ammonium degradation by AB. After that, the ratio drops because of formation of anoxic zone and AHB which reduces the oxygen consumption and the ratio reaches the minimum of ≈ 4.3 at the thickness $1.2[mm]$ and remains there until the end of the simulation, c.f. Figure 13a. The results for DN2/DA for different values of $O_\infty[gm^{-3}]$ are depicted in Figure 13b. Since formation of AHB takes time, the ratio remains constant until the biofilm reaches a specific thickness. Increasing $O_\infty[gm^{-3}]$ increases the lag time for formation of anoxic zone and AHB and DN2/DA starts increasing at approximately 0.3, 0.6, 0.8, and $1.3[mm]$ for $O_\infty = 5,\ 10,\ 15,\ 25[gm^{-3}]$ respectively. Note that since degradation of nitrate and acetate become

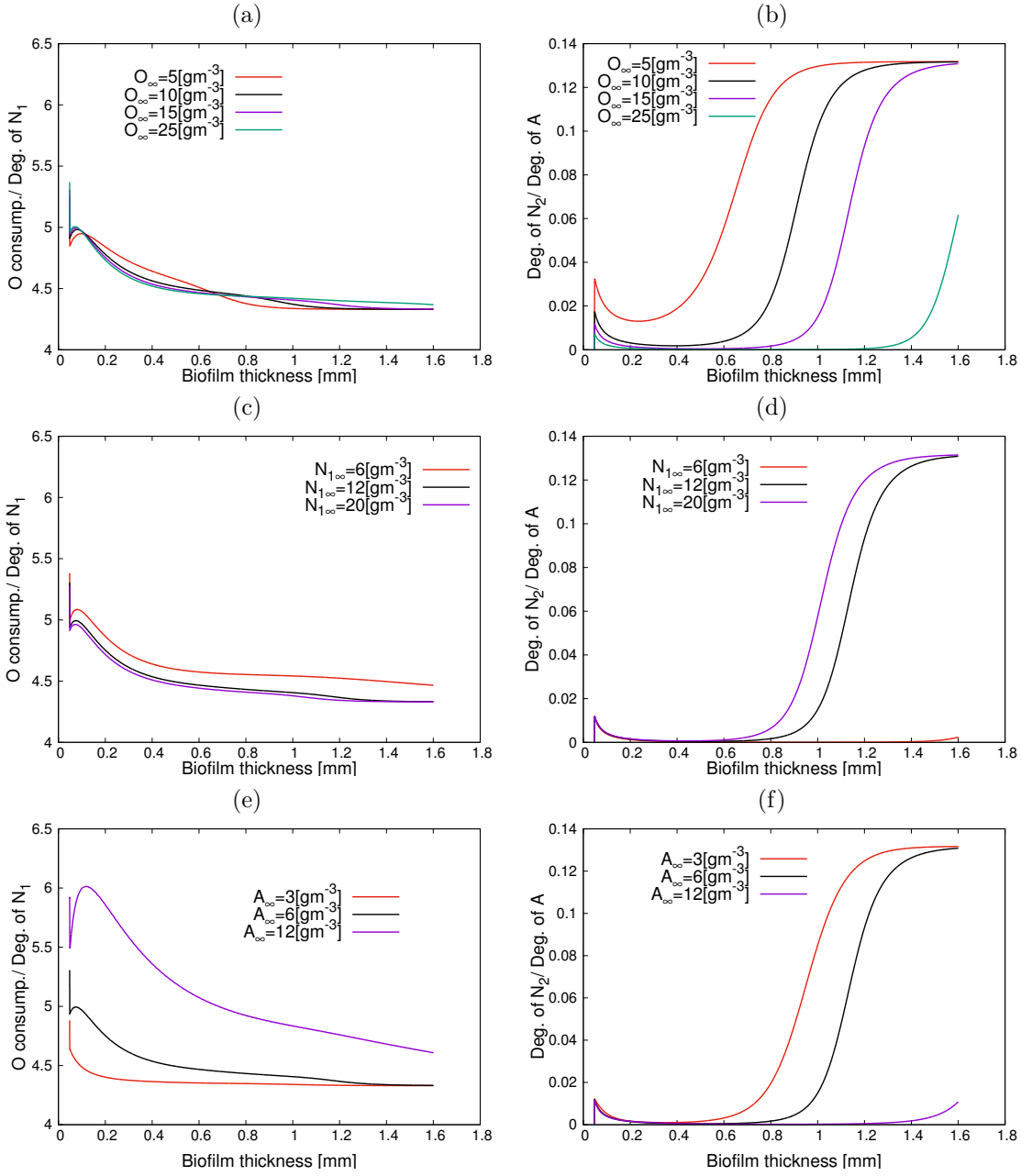

FIGURE 13. Ratio of oxygen to ammonium and nitrate to acetate consumption within the biofilm at various substrate bulk concentrations. In (a), (b) $N_{1\infty} = 12[gm^{-3}]$, $A_\infty = 6[gm^{-3}]$, in (c), (d) $O_\infty = 15[gm^{-3}]$, $A_\infty = 6[gm^{-3}]$, and in (e), (f) $N_{1\infty} = 12[gm^{-3}]$, $O_\infty = 15[gm^{-3}]$.

stable at the specific time, the ratio reaches plateau ≈ 0.13 at the thickness $0.8[mm]$, $1.2[mm]$, and $1.4[mm]$ for $O_\infty = 5$, $O_\infty = 10$, $O_\infty = 15$ respectively. Moreover because of the formation of very small amount of AHB for $O_\infty = 25[gm^{-3}]$, DN2/DA is smaller in this case and reaches ≈ 0.06 at the end of the simulation. Similar behavior is observed in the results obtained for different values

of $N_{1\infty}[gm^{-3}]$. As shown in Figure 13c, OC/DN1 initially increases and then decreases and reaches the minimum ≈ 4.6 at the biofilm thickness $1.6[mm]$ for $N_{1\infty} = 6[gm^{-3}]$ and ≈ 4.3 at the biofilm thickness $1.4[mm]$ for $N_{1\infty} = 12[gm^{-3}]$ and $N_{1\infty} = 20[gm^{-3}]$. Noteworthy here is that the ratio at $N_{1\infty} = 6[gm^{-3}]$ is higher than that at $N_{1\infty} = 12,\ 20[gm^{-3}]$ due to formation of less autotrophic bacteria which decreases the ammonium degradation. Results obtained for DN2/DA at different bulk ammonium nitrogen concentrations show that the ratio is almost zero at $N_{1\infty} = 6[gm^{-3}]$ because of the presence of more oxygen for HB which consumes acetate and inhibits formation of AHB. Increasing $N_{1\infty}[gm^{-3}]$ to 12 and $20[gm^{-3}]$ increases the ratio because of formation of less HB (due to oxygen consumption by AB) that leaves more acetate for the growth of AHB occurring at the thickness $0.8[mm]$ and $0.6[mm]$ respectively. However, in both cases the ratio reaches the plateau ≈ 0.13 at the biofilm thickness ≈ 1.5, c.f. Figure 13d. Results of the effect of $A_\infty[gm^{-3}]$ on OC/DN1 are shown in Figure 13e. At low concentration of acetate ($A_\infty = 3[gm^{-3}]$ in this study), the ratio decreases and quickly reaches the constant ≈ 4.5 due to formation of less HB that reduces the oxygen consumption and increases degradation of N_1 by AB. Increasing $A_\infty[gm^{-3}]$ results in the production of more HB which increases the ratio due to higher oxygen consumption and lower degradation of ammonium. The value of OC/DN1 increases at the beginning for $A_\infty = 6[gm^{-3}]$ and $A_\infty = 12[gm^{-3}]$ and then decreases because of oxygen depletion and reaches ≈ 4.5 and ≈ 4.8 respectively at the biofilm thickness $1.6[mm]$. Figure 13f shows the results of the impact of $A_\infty[gm^{-3}]$ on DN2/DA. Since increasing $A_\infty[gm^{-3}]$ promotes the formation of HB that inhibits production of AB and N_2 and delays the formation of AHB, the ratio is approximately zero at $A_\infty = 12[gm^{-3}]$ and increases by decreasing $A_\infty[gm^{-3}]$. It increases at the thickness $\approx 0.5[mm]$ and $\approx 0.8[mm]$ for $A_\infty = 3[gm^{-3}]$ and $A_\infty = 6[gm^{-3}]$ respectively and reaches the constant ≈ 0.13 at the end of the simulation.

Results in this section indicate that to have an optimum SND in terms of minimum oxygen consumption and maximum nitrogen removal (using the parameter values in this study), it is better to use lower concentration of O_∞, higher concentrations of $N_{1\infty}$ and medium range of A_∞. Biofilm thickness is an important factor to promote nitrification and denitrification. Using the parameter values in this study, the biofilm thickness between $\approx 0.8[mm]$ and $\approx 1.4[mm]$ is required to promote SND and the thickness $>\approx 1.4[mm]$ can be an optimum thickness to achieve an effective SND performance. Despite the positive effect of biofilm thickness on optimizing the SND performance, excessive growth of biofilm causes clogging phenomenon and results in the formation of more inert biomass that can ultimately lead to biofouling. This indicates that optimizing SND, needs a careful adjustment of involved factors that minimizes the unwanted side effects.

5. Discussion

Membrane aerated biofilm reactors (MABRs) have proven to be highly efficient biofilm technologies with tremendous potential for achieving energy and carbon-efficient simultaneous nitrification and denitrification (SND). Their unique ability to regulate substrate and oxygen distribution within biofilms through the counter-diffusion mechanism makes them promising candidates for sustainable wastewater treatment [9, 25, 29]. Mathematical modeling serves as a valuable tool to comprehend the SND mechanisms in MABRs and the influence of key process conditions. Central to modeling the performance of MABRs and SND is accurately describing biofilm development and establishing connections between biological composition, key process conditions, and SND performance. One significant aspect of biofilm growth that some theoretical studies have overlooked is that biofilms do not grow infinitely, and microbial synthesis is balanced by loss processes [19, 20, 46]. Biomass loss in biofilms can occur through detachment of cells and particles, cell lysis, hydrolysis of particles, and endogenous respiration [49]. Among these, lysis and endogenous respiration are the dominant pathways for biomass loss in biofilms

[49]. While several previous studies have considered either the cell lysis pathway or endogenous respiration to describe biomass loss and the accumulation of inert biomass [2, 6, 8, 14, 30, 33, 37, 42, 45], a limited number of studies have examined decay/lysis and endogenous respiration together as the main sources for the formation of inert biomass particularly by employing multi-scale modeling approach. Thus, our study aims to address this gap and investigate the mechanism of inert biomass accumulation within the biofilm, considering both lysis and endogenous respiration as contributing factors. Through the incorporation of cell lysis and endogenous respiration mechanisms into our 2D model, we present a more accurate description of the SND process in MABRs, accounting for the effect of inert biomass as a volume-occupying particulate within the biofilm. This comprehensive modeling approach allows us to determine optimum conditions that maximize nitrogen removal while considering the impact of inert biomass accumulation.

Our simulation results illustrate that lysis of heterotrophic bacteria (HB), anaerobic heterotrophic bacteria (AHB), and autotrophic bacteria (AB) and endogenous respiration of HB are the primary mechanisms responsible for the formation of inert biomass in the biofilm. The growth of autotrophic and heterotrophic bacteria significantly influences the amount of inert biomass formed within the biofilm, with species of higher abundances contributing more to inert biomass production as shown in Figures 8 and 10. Furthermore, our simulations demonstrate that the distributions of oxygen and acetate across the biofilm thickness differ significantly when inert biomass is considered compared to when it is neglected. This disparity further affects the distribution and abundances of HB, AB, and AHB within the biofilm, ultimately influencing the simulated SND performance of the MABR. Nevertheless, our study indicates that considering the inert biomass accumulated within the biofilm in the SND process modeling allows for more accurate identification of conditions that optimize process performance. An essential question that can be addressed through computer simulations is how key process conditions interactively affect nitrification and denitrification performance in MABRs. Our work investigates the impact of bulk concentrations of oxygen, ammonium nitrogen, and acetate on SND efficiency. Notably, we find that higher bulk concentrations of oxygen and ammonium nitrogen, along with moderate acetate concentrations, promote nitrification. Moreover, the minimum ratios of oxygen consumption to ammonia degradation (OC/DN1), which reflect oxygen consumption through nitrification, indicate that SND is most efficient at biofilm thicknesses between 1.4 to 1.6$[mm]$. This range prevents excessive HB growth due to acetate consumption by AHB during denitrification. Results of degradation of N_2/degradation of A (DN2/DA) obtained for different values of oxygen and nitrogen sources indicate that efficient denitrification occurs at the biofilm thickness $>\approx 1.4[mm]$ and it is more sensitive to environmental conditions. High oxygen bulk concentration, low ammonium nitrogen bulk concentration and very high or very low acetate bulk concentration inhibit formation of AHB and consequently removal of nitrate. Hence, based on the computer simulations in this study, SND can be achieved under conditions of $10[gm^{-3}] < O_\infty < 15[gm^{-3}]$, $12[gm^{-3}] < N_{1\infty} < 20[gm^{-3}]$, and $3[gm^{-3}] < A_\infty < 12[gm^{-3}]$ with biofilm thickness $> 1.4[mm]$. Under these conditions, the nitrogen removal rates between 0.5 to $0.85[gN/m^2/d]$ and denitrification rates between 0.01 to $0.08[gN/m^2/d]$ are achieved after ≈ 51 days ($t \approx 305$). The SND performance of MABR under various conditions has been previously studied experimentally. For example, Landes *et al.*, [25] reported the nitrification and denitrification rates of 0.15 to $0.32[gN/m^2/d]$, and 0.03 to $0.12[gN/m^2/d]$ under conditions of hydraulic retention times from 2.7 to 5.4 hours and air pressures from 24.4 to $27.8[kPa]$ ($O_\infty = 11.4$ to $11.8[gm^{-3}]$). Li and Zhang studied the impact of carbon to nitrogen ratios (C/N) on the SND performance using a pilot-scale MABR [29]. According to the reported ammonium nitrogen loading and nitrogen removal rates, nitrification rates in the range of 0.33 to $0.38[gN/m^2/d]$ and denitrification rates between 0.02 to $0.235[gN/m^2/d]$ are achieved by the pilot-scale

MABR at the C/N ratios from 2 to 8 and air pressure $0.01[MPa]$ ($O_\infty = 10.1[g/m^3]$) [29]. The nitrification and denitrification rates obtained in this study are reasonably close to the experimental results reported by Lander *et al.* [25] and Li and Zhang [29]. The discrepancies between the experimental and computational results are possibly because of varying experimental and computational conditions. Furthermore, the model used in this study does not include nitrogen removal through partial nitrification and anammox pathways and denitrification that may be caused by suspended sludge in MABRs. These simplifications can also result in the prediction of a relatively lower denitrification rate by the applied model. In addition, the results obtained by the comprehensive modeling approach in this study can be utilized for the preliminary design of an MABR. For example, for a nitrification-based MABR design, a steady-state mass balance equation for a continuous stirred-tank rector (CSTR) can be formulated as [34]:

$$QN_{1i} = R_{n1}S + QN_{1\infty}$$

where $Q[m^3d^{-1}]$ is the wastewater flow rate, $N_{1i}[gm^{-3}]$ is the ammonium nitrogen concentration in the influent, $R_{n1}[gN/m^2/d]$ is the ammonium nitrogen removal rate, $S[m^2]$ is the membrane area, and $N_{1\infty}[gm^{-3}]$ is the bulk ammonium nitrogen concentration in the reactor or effluent. Since the ammonium nitrogen degradation rate $R_{n1}[gN/m^2/d]$ can be determined by the simulation for certain $N_{1\infty}$, A_∞, and O_∞, the membrane area for the given conditions can be determined as:

$$S = \frac{QN_{1i} - QN_{1\infty}}{R_{n1}}$$

As aforementioned, an effective SND can be achieved under the conditions $10[gm^{-3}] < O_\infty < 15[gm^{-3}]$, $12[gm^{-3}] < N_{1\infty} < 20[gm^{-3}]$, and $3[gm^{-3}] < A_\infty < 12[gm^{-3}]$ with biofilm thickness $> 1.4[mm]$ in this study. However, given the generality of the biofilm model developed in this work, the proposed model can be applied to any conditions of O_∞, $N_{1\infty}$, and A_∞ to explore the SND strategies in practical MABR design. It is also worth noting that the denitrification rates that can be achieved by MABR biofilm are significantly lower than the nitrification rates under the same conditions. The main factors affecting denitrification are bulk oxygen and acetate concentrations and biofilm thickness. Nitrification and denitrification has contradictory requirement for bulk oxygen concentrations. Such contradictions can be alleviated to some extent by the increase in biofilm thickness and controlling C:N ratio in proper ranges, thanking to the counter-diffusion mass transport mechanisms in MABR. In addition, some operation strategies like intermittent aeration, are applied in MABR operation to enhance SND with MABR [4, 36, 39] which is indeed one of our future works.

6. Conclusion

In conclusion, this study presents a simulation-based exploration of the mechanisms of inert biomass accumulation within membrane aerated biofilm reactors (MABRs) and its impact on simultaneous nitrification and denitrification (SND) under diverse process conditions. By incorporating cell lysis and endogenous respiration mechanisms into our 2D model, we provide a more accurate representation of SND processes in MABRs, considering the formation of inert biomass as a volume-occupying particulate within the biofilm. This novel modeling approach enhances our understanding of SND performance and aids in determining optimal conditions to maximize nitrogen removal. Our simulation results highlight the influence of biomass loss mechanisms on substrate distribution within the biofilm. The presence of inert biomass leads to increased oxygen, ammonium nitrogen, and acetate concentrations inside the biofilm, delaying the formation of anoxic zones and the growth of anaerobic heterotrophic bacteria. Neglecting the formation of inert biomass may underestimate the required biofilm thickness for effective SND. Moreover, our simulations demonstrate the interplay of process conditions, such as bulk concentrations of oxygen, ammonium nitrogen, and acetate, on SND efficiency. Higher oxygen and ammonium

nitrogen concentrations, along with moderate acetate levels, facilitate nitrification. However, denitrification is more sensitive to environmental conditions and requires proper biofilm thickness, controlled C:N ratios, and optimized oxygen and acetate concentrations. Our study advances the knowledge of SND processes in MABRs and contributes valuable insights for designing sustainable and efficient wastewater treatment systems. As water pollution continues to pose environmental challenges, our findings support the development of SND technologies that can help preserve valuable water resources and promote environmental well-being.

References

[1] I.M. Anekwe, J. Adedeji, S. Okiemute Akpasi, S. Lewis Kiambi. *Available Technologies for Wastewater Treatment.* IntechOpen, 2022. http:/doi:10.5772/intechopen.103661.

[2] S.H. Baek, H.J. Kim. *Mathematical model for simultaneous nitrification and denitrification (SND) in membrane bioreactor (MBR) under Low Dissolved Oxygen (DO) concentrations.* Biotechnol. Bioproc. E. **18**(2013), 104–110.

[3] M.B. Benjamin. *Water Chemistry.* Waveland Press, Inc. 2010.

[4] P. Bunse, L. Orschler, S. Agrawal, S. Lackner. *Membrane aerated biofilm reactors for mainstream partial nitritation/anammox: Experiences using real municipal wastewater.* Water Res. X. **9**(2020): 100066. DOI:10.1016/j.wroa.2020.100066.

[5] F. Di Capua, F. Iannacone, F. Sabba, G. Esposito. *Simultaneous nitrification–denitrification in biofilm systems for wastewater treatment: Key factors, potential routes, and engineered applications.* Bioresour. Technol. **361**(2022): 127702.

[6] E. Casey, B. Glennon, G. Hamer. *Biofilm development in a membrane-aerated biofilm reactor: effect of flow velocity on performance.* Biotechnol. Bioeng. **67**(4)(2000), 476–86.

[7] M. Chang, B. Liang, K. Zhang, Y. Wang, D. Jin, Q. Zhang, L. Hao, T. Zhu. *Simultaneous shortcut nitrification and denitrification in a hybrid membrane aerated biofilms reactor (H-MBfR) for nitrogen removal from low COD/N wastewater.* Water Research. **211**(2022): 118027.

[8] X. Chen, P. Huo, J. Liu, F. Li, L. Yang, X. Li, W. Wei, Y. Liu, B.J. Ni. *Model predicted N2O production from membrane-aerated biofilm reactor is greatly affected by biofilm property settings.* Chemosphere. **281**(2021): 130861.

[9] T.S. Da Silva,T. Matsumoto, M.L. Dos Anjos, L.L. Albertin. *Organic matter removal in a membrane-aerated biofilm reactor.* J. Environ. Eng. **144**(2018): 04018057.

[10] H.J. Eberl, D.F. Parker, C.M. Van Loosdrecht. *A new deterministic spatio-temporal continuum model for biofilm development.* J. Theor. Med. **3**(2001), 161–175.

[11] H.J. Eberl, S. Collinson. *A modeling and simulation study of siderophore mediated antagonsim in dual-species biofilms.* Theor. Biol. Med. Mod. **6**, 30(2009).

[12] E.H. Ezechi, S.R.B.M. Kutty, M.H. Isa, A. Malakadmad, C.M. Ude, E.J. Menyechi and E. Olisa. *Determination of Decay Coefficient of Biomass through Endogenous Respiration.* Research Journal of Microbiology. **10**(8)(2015), 355–365.

[13] X. Flores-Alsina, N. Uri-Carreno, P.H. Nielsen, K.V. Gernaey. *Modelling the impacts of operational conditions on the performance of a full-scale membrane aerated biofilm reactor.* Science of The Total Environment. **856**(2023): 158980.

[14] M. Friedrich, I. Takács. *A new interpretation of endogenous respiration profiles for the evaluation of the endogenous decay rate of heterotrophic biomass in activated sludge.* Water Research. **47**(15)(2013), 5639–5646.

[15] M.R. Frederick, C. Kuttler, B.A. Hense, H.J. Eberl. Â mathematical model of quorum sensing regulated EPS production in biofilms. Theor. Biol. Med. Mod. **8**(2011), 1-29.

[16] M. Ghasemi, S. Sonner, H.J. Eberl. *Time adaptive numerical solution of a highly nonlinear degenerate cross-diffusion system arising in multi-species biofilm modeling.* Eur. J. Appl. Math. **29**(2018), 1035–1061.

[17] M. Ghasemi, H.J. Eberl. *Time adaptive numerical solution of a highly degenerate diffusion-reaction biofilm model based on regularisation.* J. Sci. Comp. **74**(2018), 1060–1090.

[18] M. Ghasemi, B.A. Hense, H.J. Eberl, C. Kuttler. *Simulation-Based Exploration of Quorum Sensing Triggered Resistance of Biofilms to Antibiotics.* Bull. Math. Biol. **80**(7)(2018), 1736–1775.

[19] M. Ghasemi, S. Chang, H.J. Eberl. *Simulation of composition and mass transfer behaviour of a membrane biofilm reactor using a two dimensional multi-species counter-diffusion model.* J. Membr. Sci. **618**(2021): 118636.

[20] M. Ghasemi, S. Chang, S. Sivaloganathan. *Modeling and simulation study of simultaneous nitrification–denitrification in membrane aerated bioreactor.* J. Membr. Sci. **668**(2023): 121210.

[21] M. Gonzalez-Brambila, O. Monroy, F. Lopez-Isunza. *Experimental and theoretical study of membrane-aerated biofilm reactor behaviour under different modes of oxygen supply for the treatment of synthetic wastewater.* Chemical Engineering Science. **61**(2006), 5268–5281.

[22] M. Henze, W. Gujer, T. Matsuo, M.C.M. van Loosdrecht. *Activated sludge models ASM1, ASM2, ASM2d and ASM3. Scientific and Technical Reports.* IWA publishing, 2000.

[23] H. Khassehkhan, T. Hillen, H.J. Eberl. *A non-linear master equation for a degenerate diffusion model of biofilm growth.* LNCS. **5544**(2009), 735–744.

[24] J.-U. Kreft,J.W.T. Wimpenny. *Effect of EPS on biofilm structure and function as revealed by an individual-based model of biofilm growth.* Water Sci. Technol. **43**(2001),135–141.

[25] N. Landes, A. Rahman, A. Morse, W.A. Jackson. *Performance of a lab-scale membrane aerated biofilm reactor treating nitrogen dominant space-based wastewater through simultaneous nitrification-denitrification.* J. of Environ. Chem. Eng. **9**(2021): 104644.

[26] C.S. Laspidou, B.E. Rittmann. *Modeling the development of biofilm density including active bacteria, inert biomass, and extracellular polymeric substances.* Water Research. **38**(2004), 3349–3361.

[27] M. Lan, P. Yang, L. Xie, Y. Li, J. Liu, P. Zhang, P. Zhang, B. Li. *Start-up and synergistic nitrogen removal of partial nitrification and anoxic/aerobic denitrification in membrane aerated biofilm reactor.* Environmental Research. **214**(2022): 113901.

[28] M. Li, C. Du, J. Liu, X. Quan, M. Lan, B. Li. *Mathematical modeling on the nitrogen removal inside the membrane-aerated biofilm dominated by ammonia-oxidizing archaea (AOA): effects of temperature, aeration pressure and COD/N ratio.* Chemical Engineering Journal. **338**(2018), 680–687.

[29] Y. Li, k. Zhang. *Pilot scale treatment of polluted surface waters using membrane aerated biofilm reactor (MABR).* Biotechnol. Biotechnol. Equip. **32**(2018), 376–386.

[30] Y. Liu, T. Zhu, S. Ren, T. Zhao, H. Chai, Y. Xu, L. Peng, Y. Liu. *Contribution of nitrification and denitrification to nitrous oxide turnovers in membrane-aerated biofilm reactors (MABR): A model-based evaluation.* Science of The Total Environment. **806**(2022): 151321.

[31] J.E. Macias-Diaz. *A positive finite-difference model in the computational simulation of complex biological film models.* J. Differ. Equ. Appl. **20**(4)(2014), 548–569.

[32] K.J. Martin, R. Nerenberg. *The membrane biofilm reactor (MBfR) for water and wastewater treatment: principles, applications, and recent developments.* Bioresour. Technol. **122**(2012), 83–94.

[33] S. Matsumoto, A. Terada, S. Tsuneda. *Modeling of membrane-aerated biofilm: Effects of C/N ratio, biofilm thickness and surface loading of oxygen on feasibility of simultaneous nitrification and denitrification.* Biochem. Eng. J. **37**(2007), 98–107.

[34] A. Masic. *Investigation of a biofilm reactor model with suspended biomass.* Doctoral Theses in Mathematical Sciences, Lund University, 2013.

[35] A. Masic, H.J. Eberl. *On optimization of substrate removal in a bioreactor with wall attached and suspended bacteria.* Math. Biosc. Eng. **11**(5)(2014), 1139–1166.

[36] S. Mehrabi, D. Houweling, M. Dagnew. *MABR process development downstream of a carbon redirection unit: opportunities and challenges in nitrogen removal processes.* Environmental Technology. **44**(26)(2023), 4084–4097.

[37] P. Mei, Z. Wang, W. Guo, Y. Gao, P.A. Vanrolleghem, Y. Li. *The ASM2d model with two-step nitrification can better simulate biological nutrient removal systems enriched with complete ammonia oxidizing bacteria (comammox Nitrospira).* Chemosphere. **335**(2023): 139169.

[38] S. Murshid, A. Antonysamy, G. Dhakshinamoorthy, A. Jayaseelan, A. Pugazhendhi. *A review on biofilm-based reactors for wastewater treatment: Recent advancements in biofilm carriers, kinetics, reactors, economics, and future perspectives.* Science of The Total Environment. **892**(2023): 164796.

[39] C. Pellicer-Nàcher, S. Sun, S. Lackner, A. Terada, F. Schreiber, Q. Zhou, B.F. Smets. *Sequential Aeration of Membrane-Aerated Biofilm Reactors for High-Rate Autotrophic Nitrogen Removal: Experimental Demonstration.* Environ. Sci. Technol. **44**(2010), 7628–7634.

[40] K.A. Rahman, S. Sonner, H.J. Eberl. *Derivation of a multi-species cross-diffusion model from a lattice differential equation and positivity of solutions.* Acta Phys. Pol. B. **9**(1)(2016), 121–132.

[41] J. Rang. *Improved traditional Rosenbrock-Wanner methods for stiff ODEs and DAEs.* Journal of Computational and Applied Mathematics. **286**(2015), 128–144.

[42] M. Revilla, B. Galán, J.R. Viguri. *An integrated mathematical model for chemical oxygen demand (COD) removal in moving bed biofilm reactors (MBBR) including predation and hydrolysis.* Water Research. **98**(2016), 84–97.

[43] B.E. Rittmann. *The membrane biofilm reactor is a versatile platform for water and wastewater treatment.* Environ. Eng. Res. **12**(2007), 157–175.

[44] F. Sabba, C. Picioreanu, J.P. Boltz, R.J.W.S. Nerenberg. *Predicting N2O emissions from nitrifying and denitrifying biofilms: A modeling study.* Water Sci. Technol. **75**(3-4)(2017), 530–538.

[45] M. Sarioglua, G. Insel, N. Artanb, D. Orhon. *Model evaluation of simultaneous nitrification and denitrification in a membrane bioreactor operated without an anoxic reactor.* J. Membr. Sci. **337**(2009), 17–27.

[46] M. Seifi, M.H. Fazaelipoor. *Modeling simultaneous nitrification and denitrification (SND) in a fluidized bed biofilm reactor.* App. Math. Model. **36**(2012), 5603–5613.

[47] A. Terada, K. Hibiya, J. Nagai, S. Tsuneda, A. Hirata. *Nitrogen removal characteristics and biofilm analysis of a membrane-aerated biofilm reactor applicable to high-strength nitrogenous wastewater treatment.* J. Biosci. Bioeng. **95**(2003), 170–178.

[48] Mark.C.M. Van Loosdrecht, M. Henze. *Maintenance, endogeneous respiration, lysis, decay and predation.* Water Science and Technology. **39**(1)(1999), 107–117.

[49] O. Wanner, H.H. Eberl, M.C.M. Van Loosdrecht, E. Morgenroth, D.R. Noguera, C. Picioreanu, B.E. Rittmann. *Mathematical Modelling of Biofilms.* IWA Publishing, 2006.

[50] X. Xu, H. Yang, C. Li. *Theoretical model and actual characteristics of air pollution affecting health cost: A review.* Int. J. Environ. Res. Public Health. **19**(6)(2022):3532.

M. Ghasemi, corresponding author, Department of Applied Mathematics, University of Waterloo, Waterloo, ON, Canada N2L 3G1

Email address: m23ghase@uwaterloo.ca

S. Chang, School of Engineering University of Guelph, Guelph, ON, Canada, N1G 2W1

Email address: schang01@uoguelph.ca

S. Sivaloganathan, Department of Applied Mathematics, University of Waterloo, Waterloo, ON, Canada N2L 3G1

Email address: ssivaloganathan@uwaterloo.ca